Accepted Manuscript

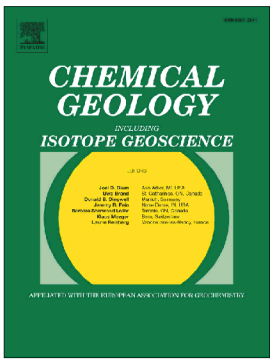

Water mass transformation in the Barents Sea inferred from radiogenic neodymium isotopes, rare earth elements and stable oxygen isotopes

Georgi Laukert, Mikhail Makhotin, Mariia V. Petrova, Martin Frank, Ed C. Hathorne, Dorothea Bauch, Philipp Böning, Heidemarie Kassens

PII: S0009-2541(18)30497-2
DOI: doi:10.1016/j.chemgeo.2018.10.002
Reference: CHEMGE 18935

To appear in: *Chemical Geology*

Received date: 18 May 2018
Revised date: 10 August 2018
Accepted date: 3 October 2018

Please cite this article as: Georgi Laukert, Mikhail Makhotin, Mariia V. Petrova, Martin Frank, Ed C. Hathorne, Dorothea Bauch, Philipp Böning, Heidemarie Kassens , Water mass transformation in the Barents Sea inferred from radiogenic neodymium isotopes, rare earth elements and stable oxygen isotopes. Chemge (2018), doi:10.1016/j.chemgeo.2018.10.002

Water mass transformation in the Barents Sea inferred from radiogenic neodymium isotopes, rare earth elements and stable oxygen isotopes

Georgi Laukert [a,*], Mikhail Makhotin [b], Mariia V. Petrova [a,c,d], Martin Frank [a], Ed C. Hathorne [a], Dorothea Bauch [a], Philipp Böning [e], and Heidemarie Kassens [a]

[a] GEOMAR Helmholtz Centre for Ocean Research Kiel, Wischhofstr. 1-3, 24148 Kiel, Germany

[b] AARI, Arctic and Antarctic Research Institute, ul. Beringa 38, Saint Petersburg, Russia

[c] Aix Marseille Université, CNRS/INSU, Université de Toulon, IRD, Mediterranean Institute of Oceanography (MIO) UM 110, 13288 Marseille, France

[d] Saint Petersburg State University, 7/9 Universitetskaya Emb., 199034, Saint Petersburg, Russia

[e] Max Planck Research Group for Marine Isotope Geochemistry, Institute for Chemistry and Biology of the Marine Environment (ICBM), University of Oldenburg, Carl-von-Ossietzky-Str. 9-11, 26129 Oldenburg, Germany

[*] Corresponding author at: GEOMAR Helmholtz Centre for Ocean Research Kiel, Wischhofstr. 1-3, 24148 Kiel, Germany. Tel.: +49 431 600 2254 / 2888. E-mail address: glaukert@geomar.de.

Key words:

Arctic Ocean; Barents Sea; neodymium isotopes; rare earth elements; water masses; scavenging

Highlights:

- First comprehensive seawater Nd isotope and REE data set for the Barents Sea.
- Water masses traced with Nd isotopes, salinity and stable oxygen isotopes.
- No release of particulate REEs to the dissolved load except for cerium.
- Transformation of Atlantic Water accompanied by pronounced REE removal from the dissolved phase.

ABSTRACT

Nearly half the inflow of warm and saline Atlantic Water (AW) to the Arctic Ocean is substantially cooled and freshened in the Barents Sea, which is therefore considered a key region for water mass transformation in the Arctic Mediterranean. Numerous studies have focused on this transformation and the increasing influence of AW on Arctic climate and biodiversity, yet geochemical investigations of these processes have been scarce. Using the first comprehensive data set of the distributions of dissolved radiogenic neodymium (Nd) isotopes (expressed as ε_{Nd}), rare earth elements (REE) and stable oxygen isotope ($\delta^{18}O$) compositions from this region we are able to constrain the transport and transformation of AW in the Barents Sea and to investigate which processes change the chemical composition of the water masses beyond what is expected from circulation and mixing.

Inflowing AW and Norwegian Coastal Water (NCW) both exhibit distinctly unradiogenic ε_{Nd} signatures of -12.4 and -14.5, respectively, whereas cold and dense Polar Water (PW) has considerably more radiogenic ε_{Nd} signatures reaching up to -8.1. Locally formed Barents Sea Atlantic Water (BSAW) and Barents Sea Arctic Atlantic Water

(BSAAW) are encountered in the northeastern Barents Sea and have intermediate ε_{Nd} values resulting from admixture of PW containing small amounts of riverine freshwater from the Ob (< ~1.1 %) to AW and NCW. Similar to the Laptev Sea, the dissolved Nd isotope composition in the Barents Sea seems to be mainly controlled by water mass advection and mixing despite its shallow water depth. Strikingly, the BSAW and BSAAW are marked by the lowest REE concentrations reaching 11 pmol/kg for Nd ([Nd]), which in contrast to the Nd isotopes, cannot be attributed to the admixture of REE-rich Ob freshwater to AW or NCW ([Nd] = 16.7, and 22 pmol/kg, respectively) and instead reflects REE removal from the dissolved phase with preferential removal of the light over the heavy REEs. The REE removal is, however, not explainable by estuarine REE behavior alone, suggesting that scavenging by (re)suspended (biogenic) particles occurs locally in the Barents Sea. Regardless of the exact cause of REE depletion, we show that AW transformation is accompanied by geochemical changes independent of water mass mixing.

1. INTRODUCTION

Over the past 30 years, the volume of warm and saline Atlantic Water (AW) present in the Barents Sea (BS) has more than doubled at the expense of Arctic-derived cold and fresh Polar Water (PW) (Oziel et al., 2016). The enhanced advection of warm AW has been regarded the main driver of the marked sea-ice retreat observed in the BS (Årthun et al., 2012) and more recently also in the Eurasian Basin of the Arctic Ocean (AO) (Polyakov et al., 2017). Among the Arctic regions the BS has experienced the strongest sea-ice loss in winter (Onarheim et al., 2018), which is consistent with the growing impact of oceanic heat loss. The exact causal relationship between increasing AW inflow and decreasing sea-ice extent is still under debate but the overall change to more temperate conditions in the Eurasian part of the Arctic through increased influence of AW on the upper water column is well documented. In fact, due to the extensive sets of hydrographic data (S, T, density and nutrients) collected over the last

decades, the hydrography and dynamics of the BS are amongst the best known of the Arctic shelf seas (cf. Korablev et al., 2014; Oziel et al., 2016). The ongoing "Atlantification" of the AO is accompanied by an alteration of the marine ecosystems, which in the BS is mainly reflected by a shift in spring and summer phytoplankton blooms to the Northeast (Oziel et al., 2017) and an increase in the amount of krill (Eriksen et al., 2017). The BS accounts for ~40 % of the primary productivity of the Arctic shelf regions (Ardyna et al., 2013; Arrigo and van Dijken, 2015; Sakshaug, 2004), such changes thus are expected to have broad implications for the marine ecosystem state of the entire AO.

In contrast to the significant progress made in oceanographic and biological research, little is known about the (bio)geochemical processes affecting the chemical composition of the water column in the BS and their response to the observed recent changes. This is because only limited trace metal and rare earth element (REE) data are available from this region. In detail, no comprehensive trace metal concentration data have been obtained from the BS to date and concentrations and radiogenic isotope compositions of the REE neodymium (Nd) have so far only been reported for seawater collected at one station in the northwestern BS (Andersson et al., 2008). However, in other regions of the Arctic Mediterranean (i.e. the Arctic Ocean and the Nordic Seas) the Nd isotope system has been successfully applied as a tracer of water mass circulation and mixing (Andersson et al., 2008; Charette et al., 2016; Lacan and Jeandel, 2004a, b; Laukert et al., 2017a, b, c; Porcelli et al., 2009; Zimmermann et al., 2009). This isotope system is characterized by slow decay of the samarium (Sm) isotope ^{147}Sm to the radiogenic Nd isotope ^{143}Nd, whose ingrowth together with the differentiation of Sm and Nd during partial melting or fractional crystallization cause characteristic $^{143}Nd/^{144}Nd$ ratios of rocks. These specific signatures vary as a function of rock age and lithology and are commonly expressed as ε_{Nd}, which denotes the deviation of a measured $^{143}Nd/^{144}Nd$ ratio from the 'Chondritic Uniform Reservoir' (CHUR) ratio of 0.512638 in parts per 10000 (Jacobsen and Wasserburg, 1980). The ε_{Nd} signatures of rocks are introduced into the oceans

via riverine or aeolian inputs of weathered continental material and are subsequently advected and preserved in water masses of the open ocean due to the quasi-conservative behavior of Nd (Frank, 2002; Goldstein and Hemming, 2003) and its intermediate average oceanic residence time of several hundred years (Arsouze et al., 2009; Rempfer et al., 2011; Tachikawa et al., 2003). Apart from water mass circulation and mixing, water mass ε_{Nd} signatures can only be modified through seawater-particle interactions occurring either within the water column or at the land-ocean boundaries (e.g. Abbott et al., 2015a, b; Jeandel, 2016; Johannesson and Burdige, 2007; Johannesson et al., 2017; 2011; Lacan and Jeandel, 2001; 2005; Nozaki and Alibo, 2003; Siddall et al., 2008). The Nd isotope system therefore not only has a high potential for providing important information beyond that deducible from hydrographic parameters, but recently has also become a useful tool to determine REE fluxes between the different pools present in seawater and marine sediments.

In the open Arctic Mediterranean, the seawater Nd isotope distribution can generally be explained by water mass circulation and mixing (Andersson et al., 2008; Lacan and Jeandel, 2004a, b; Laukert et al., 2017a, c; Porcelli et al., 2009; Zimmermann et al., 2009). Seawater-particle interactions change the dissolved Nd isotope compositions only on the North-East Greenland Shelf (Laukert et al., 2017a) and in the Chukchi Sea (Charette et al., 2016; Dahlqvist et al., 2007; Porcelli et al., 2009), whereas on the vast Siberian shelves such interactions are dominated by removal of riverine REEs and no significant REE release from particulate phases or any associated change in the seawater Nd isotope composition is observed (Laukert et al. 2017b). As shown in Figure 1, the REE budget of the Arctic Mediterranean is dominated by AW, which is characterized by ε_{Nd} signatures of -13 and -12.6 at the Iceland-Scotland Ridge and the Denmark Strait, respectively (Laukert et al., 2017a and references therein). Pacific-derived waters entering the AO through the Bering Strait have distinctly more radiogenic ε_{Nd} signatures around -2 to -3 (Charette et al., 2016), which are altered close to the Bering Strait via seawater-particle interactions resulting in ε_{Nd} values near

-5.5 for modified Pacific-derived waters entering the AO through the Chukchi Sea (Dahlqvist et al., 2007, Porcelli et al., 2009). The Norwegian Coastal Water (NCW) is another important source for the marine REE budget of the Arctic Mediterranean and is characterized by an ε_{Nd} signature of -14.5 in the southern BS (Laukert et al., 2017a; this study). The discharge of freshwater from the different Arctic rivers is characterized by a wide range of Nd concentrations and isotope compositions (Laukert et al., 2017a, b; Persson et al., 2011; Porcelli et al., 2009; Zimmermann et al., 2009). Additional contributions of REEs via glacial meltwater and runoff are generally confined to the shelf regions of Greenland (e.g. Lacan and Jeandel, 2004a; Laukert et al., 2017a), whereas aeolian inputs have not been reported to date but will likely only be of limited importance for permanently and seasonally ice-covered areas.

In this study we present dissolved radiogenic Nd isotope compositions, dissolved REE concentrations and stable oxygen isotope compositions together with hydrographic data to refine the knowledge on the transport and transformation of AW in the BS and to identify (bio)geochemical processes occurring in the water column. The data reported here were obtained from samples collected in 2014 in the central and northeastern BS and besides a refinement of the water mass components and their distribution indicate that AW transformation is associated with a pronounced removal of dissolved REEs.

2. HYDROGRAPHIC SETTING

Compared to the freshwater-dominated Siberian Arctic seas the BS is characterized by high salinities (S > ~30) resulting from the inflow of relatively warm and saline AW and comparatively little river runoff (Fig. 1). The volume transport of AW across the BS amounts to ~2 Sverdrup (Sv) (Skagseth, 2008), which corresponds to approximately ~40 % of the total AW inflow into the AO considering an AW volume flux of ~3.2 Sv via the eastern Fram Strait (Mauritzen et al., 2011). The AW inflow is complemented by the inflow of NCW,

which originates in the Baltic Sea (Björk et al., 2001; Gascard, 2004) and is advected into the southern BS via the Norwegian Coastal Current (Loeng, 1991). The volume transport of NCW is ~1.8 Sv (Skagseth et al., 2011), which is similar to that of AW entering the AO via the BS.

The advection of AW into the Arctic Mediterranean (i.e. AO and Nordic Seas) is an integral part of the Atlantic thermohaline overturning circulation, which in the BS is represented by AW transformation into colder and denser water and which from there on is referred to here as Barents Sea Atlantic Water (BSAW). The BSAW flows eastwards across the passage between Novaya Zemlya and Franz Josef Land and mainly enters the deep AO through the St. Anna Trough (e.g. Loeng, 1991). The formation and admixture of BS-derived waters to the intermediate layers of the open AO is well documented (e.g. Dmitrenko et al., 2009; Lien and Trofimov, 2013; Lind et al., 2016; Oziel et al., 2016). However, most of the observational research conducted over the last few decades focused on the western and central part of the BS, while the northeastern part including the region between Novaya Zemlya and Franz Josef Land is still comparably understudied due to difficult ice conditions prevailing there most of the year. Latest research efforts investigating the hydrography in this region indicate that exchange between the open AO and the northern BS is more complex than previously suggested, in particular due to the previously unconsidered presence of Arctic Atlantic Water (AAW) entering the BS from the Kara Sea (Makhotin and Ivanov, 2016). The factors controlling temporal changes in the advection and distribution of AW in the BS are also subject of ongoing research. Variability in AW advection has been attributed to changing atmospheric patterns (e.g. Ingvaldsen et al., 2004; Proshutinsky and Johnson, 1997) and more recently has also been linked to the Atlantic Multi-Decadal Oscillation (Levitus et al., 2009), whereby overall warming of waters was observed in different regions north of 60 °N (Seidov et al., 2015). Understanding the role of atmospheric interannual variability in controlling AW advection remains challenging due to the fact that temperature, salinity and density

characteristics are decoupled in the BS during AW transformation. This is because salinity anomalies are mainly established and sustained by horizontal advection, while temperature anomalies are subject to air-sea interactions resulting in their separate propagation (Yashayaev and Seidov, 2015).

3. METHODS

The samples of this study were recovered between 1st and 29th June 2014 aboard the Russian research vessel RV Professor Molchanov in the frame of the Russian project "Arctic Floating University". Continuous CTD (conductivity, temperature, depth) profiles were obtained in the central BS along a latitudinal transect between 70.0 °N and 79.3 °N at approximately 33.5 °E, and in the eastern BS along several transects between Novaya Zemlya and Franz Josef Land. For the recovery of all seawater samples along the transects a rosette water sampler equipped with a SBE19plus CTD and Niskin-type sample bottles was used.

Oxygen isotope compositions were analyzed at the Stable Isotope Laboratory of the College of Earth, Ocean, and Atmospheric Sciences at Oregon State University (Corvallis, USA) applying a CO_2-water isotope equilibration technique (Epstein and Mayeda, 1953) on at least two subsamples on a DeltaPlusXL instrument at an external reproducibility of ±0.04 ‰ or better. The measured $^{18}O/^{16}O$ ratios are provided as deviation from Vienna Standard Mean Ocean Water in the δ-notation (Craig, 1961). Sample salinity (S_m) was determined with an AutoSal 8400A salinometer at GEOMAR with a precision of ±0.003 and an accuracy better than ±0.005. The S and $\delta^{18}O$ data were combined to determine the fractions (f) of meteoric water (which is essentially only riverine freshwater, RF, given that precipitation can be neglected), sea-ice meltwater (SIM; negative values are proportional to the subsequent addition of brines to the water column) and marine water (SW) by applying mass balance equations (Östlund and Hut, 1984). The end-member values for SIM were taken from Bauch and Cherniavskaia (2018) and those for SW were calculated by averaging the values of AW

samples of this study (S = 35.02, $\delta^{18}O$ = 0.3, n = 6). For RF, a $\delta^{18}O$ value of -15.5 ‰ was adopted from Dubinina et al. (2017) representing freshwater discharged into the Kara Sea. Following Laukert et al. (2017b), we use S_m and $\delta^{18}O$ to determine the initial salinity S_0, which is the expected salinity without contributions from sea-ice formation and melting. Nutrient concentrations (silicate and phosphate) were analyzed on board following standard procedures (Grasshoff et al., 2009).

For Nd isotope and REE concentration analyses 10 L of seawater were directly filtered through AcroPak^{TM}500 Capsules with Supor Membrane (pore size: 0.8/0.2 µm) filter cartridges and collected in acid-cleaned LDPE containers. After transport to the Otto-Schmidt Laboratory in St. Petersburg, Russia, the samples were acidified to pH ~2.2 with ultra-pure concentrated HCl and aliquots of 1 L were separated into acid-cleaned LDPE-bottles for concentration analyses. About 100 mg of Fe were added to the remaining large volume of the samples as a purified $FeCl_3$ solution and after equilibration for 48 hours the pH was adjusted to ~8 leading to co-precipitation of the dissolved REEs with FeOOH. The supernatant was discarded and the Fe-precipitates were transferred into 1 L acid-cleaned LDPE-bottles for further treatment in the home laboratory at GEOMAR. After pre-concentration and evaporation, the samples were treated with aqua regia at 110 °C for at least 24 h to destroy organic components. Precleaned diethyl ether was then used to separate the Fe from the samples following Stichel et al. (2012). Further separation of the major element cations and high field strength elements from the REEs was achieved through cation exchange chromatography (BIORAD® AG50W-X8 resin, 200-400 µm mesh-size, 1.4 mL resin bed) following the separation scheme of Barrat et al. (1996). Neodymium was then purified by a second column chemistry step using Eichchrom® LN-Spec resin (50-100 µm mesh size, 2 mL resin bed) and a modified separation scheme of Le Fèvre and Pin (2005) and Pin and Zalduegui (1997). Finally, the samples were treated with H_2O_2 (~30 wt.%) for at least 2 hours to avoid possible contamination by traces of resin and to prevent disturbing matrix effects.

The Nd isotope compositions were measured on a Neptune Plus (Thermo Scientific) MC-ICP-MS at the ICBM (University of Oldenburg) and a Nu Plasma (Nu Instruments Limited) at GEOMAR. For correction of instrumental mass bias an exponential mass fractionation was applied using a $^{146}Nd/^{144}Nd$ ratio of 0.7219 and the measured $^{143}Nd/^{144}Nd$ sample ratios were normalized to the accepted value of 0.512115 for the JNdi-1 standard (Tanaka et al., 2000). The 2σ external reproducibility ranged between 0.2 and 0.4 ε_{Nd} units for the individual measurement runs based on repeated measurements of JNdi-1 and in-house standards with concentrations similar to those of the samples.

The REE concentrations were determined using an online pre-concentration (OP) ICP-MS technique at GEOMAR by directly coupling a "seaFAST" system (Elemental Scientific Inc., Nebraska, USA) to an ICP-MS (Agilent 7500ce) (Hathorne et al., 2012). This method was recently improved by using an 8 ml sample loop and calibration standards with a mixed REE solution of a seawater-like composition in a natural seawater matrix (see also Osborne et al., 2015). Repeated measurements of GEOTRACES inter-calibration sample BATS 15m (van de Flierdt et al., 2012) were used to monitor the external reproducibility. Neodymium concentrations were in addition determined using an isotope dilution (ID) method following Rickli et al. (2009). In brief, a pre-weighed ^{150}Nd spike was added to 0.5 L of each sample and sufficient time was given for equilibration. After addition of the purified $FeCl_3$ solution, co-precipitation was achieved at pH ~8. Pre-concentration and REE separation was then performed identically to that of the large volume samples (see above), except that only the cation exchange chromatography (BIORAD® AG50W-X8 resin, 200-400 μm mesh-size, 1.4 mL resin bed) was applied.

The entire pre-concentration, purification and measurement techniques regarding the determination of Nd isotopes and REE concentrations strictly followed approved GEOTRACES protocols and were confirmed through participation in the international GEOTRACES intercalibration study (van de Flierdt et al., 2012).

4. RESULTS

All Nd isotope, REE concentration and $\delta^{18}O$ data presented here are reported in table 1 together with corresponding hydrographic information, and in addition are accessible through the PANGAEA database (LINK WILL BE PROVIDED ONCE THIS MS WILL BE ACCEPTED). The complete hydrographic data set of our study has previously been discussed by Makhotin and Ivanov (2016) along with hydrographic data from 2012 and 2013 and all data are accessible through the PANGAEA database (LINK WILL BE PROVIDED BY MAKHOTIN ET AL. ONCE THE MS WILL BE ACCEPTED). Water masses were mainly classified based on the basis of constant θ-S end-member definitions after Rudels et al. (2012; 2005). However, this classification had to be extended to the regional hydrography by slightly adjusting the θ-S properties and by adding locally present water masses according to observations made in this study and based on literature results (Harris et al., 1998; Lien and Trofimov, 2013; Loeng, 1991; Makhotin and Ivanov, 2016; Oziel et al., 2016; Pfirman et al., 1994). The θ-S characteristics of the water masses are reported in table 2 along with their Nd isotope and REE signatures. We note that our θ-S definitions of the water masses slightly differ from those suggested by Oziel et al. (2016) who recently provided a comprehensive assessment of the BS hydrography and water mass dynamics as well as their changes over the last 30 years. Our classification, however, mainly aims at a better understanding of the distribution of the tracers applied in this study and is not supposed to be fully comparable with previous hydrographic studies.

4.1 Hydrography and water masses based on $\delta^{18}O$ and S

Overall a relatively narrow range in S ($33.5 < S_m < 35$) but strong temperature gradients ($-2 < \theta < 6$ °C) are observed for the waters circulating in the BS. In θ-S space, warm ($\theta > 4$ °C) and relatively fresh ($S_m < 34.9$) NCW clearly is separated from colder ($\theta < 0$ °C) but similarly

fresh PW through the presence of relatively warm (~0 < θ < 4.5 °C) and saline (S_m > 35) AW (Fig. 2). In contrast to AW and PW that both exhibit a wide vertical and horizontal spread (see Figs. 3 and 4), the NCW based on θ-S properties is encountered only in the upper water column (< 150 m) of the southern BS (south of 72 °N). The ~400 km wide body of AW is located further north (centered at ~74 °N) and is marked by constant S_m (~35) throughout the water column but comprises variable temperatures that generally decrease towards the north (Figs. 3 and 4).

In the northeastern BS, temperatures near zero and S_m ranging between 34.90 and 34.95 indicate the presence of BSAW at 50 to 250 m depth along the northwestern slope of Nowaya Zemlya (at ~75-77 °N) (Fig. 4). A water mass with similar θ-S characteristics is located further north (mainly at ~79 °N) spreading below 150 m depth (Fig. 4). Hydrographic data from 2012 and 2013 obtained further to the East indicate that this water is the transformed continuation of relatively warm (up to ~1.4 °C in 2013) AAW advected from the open AO through the Kara Sea via the St. Anna Trough (Makhotin and Ivanov, 2016). These waters were significantly colder (below 0 °C) in 2014 compared to the AAW observed in 2012 and 2013 further east, suggesting that substantial cooling must have occurred during AAW transport across the northeastern BS. Therefore, we distinguish between the precursor AAW circulating in the open AO or the Kara Sea and the transformed AAW in the BS by referring to the latter as Barents Sea Arctic Atlantic Water (BSAAW). The BSAAW is observed as far north as 79.5 °N (e.g. at the southern end of Franz Victoria Through) and to the south separated from BSAW by a ~100 km wide and ~150 m deep body of cold and less saline PW (Fig. 4). Waters comprising the latter generally have lowest temperatures at 50 to 200 m depth (θ ~ -2 °C), while at the surface they are marked by somewhat higher temperatures (θ reaching ~0 °C). In the northernmost BS close to Spitsbergen they are identifiable by the lowest S_m (reaching ~33.5) of the data set (Fig. 4).

The overall ranges in f_{RF} and f_{SIM} are low but significant to identify differences for the individual water masses. While the $\delta^{18}O$ and S_m values of samples representing the core of AW were used to determine the SW end-member and thus the f_{RF} of AW is set to zero by definition, samples representing NCW, PW and BS(A)AW are marked by higher f_{RF} values reaching 1.1 % for PW (Fig. 2). Only one sample representing PW (station 54, 11 m) has exceptionally low f_{RF} compared to what can be expected based on its S_m value (Fig. 2). This sample also has the highest f_{SIM} of the data set (~2.7 %), which together with the low f_{RF} suggests that its lowered S_m resulted from addition of sea-ice meltwater rather than river water. No correlation is found between f_{RF} and f_{SIM} for PW or any other water mass and essentially all samples have positive f_{SIM} suggesting the absence of significant brine contribution. The $\delta^{18}O$-based parameters do also not correlate with nutrient concentrations, which generally are depleted at the surface and increase with depth.

4.2 Nd isotopes, REE concentrations and REE distribution patterns

As shown in Figure 5a, the separation of NCW from PW observed in θ-S space (section 4.1) is also reflected by the distribution of the REE concentrations (here represented by the Nd concentration determined via isotope dilution, i.e. $[Nd]_{ID}$). Samples reflecting NCW have the highest dissolved REE concentrations at an average $[Nd]_{ID}$ of 22.5 pmol/kg (1 SD = 0.3, n = 2), whereas the average $[Nd]_{ID}$ of AW samples collected further north is significantly lower at 16.6 pmol/kg (1 SD = 1.3, n = 5) (see also Fig. 2). Three samples that cannot clearly be attributed to either NCW or AW but have θ-S characteristics intermediate between these water masses and hence are termed AW-NCW (Fig. 5). Samples obtained from the northeastern BS with θ-S characteristics of PW have slightly more variable but generally lower REE concentrations than AW and NCW. As shown in Figures 2 and 5, the lowest $[Nd]_{ID}$ were found in BSAAW reaching 11 pmol/kg for the deepest sample of the entire data set (station 126, 350 m).

The general trends observed for $[Nd]_{ID}$ apply to all dissolved REEs, yet different gradients are found for each REE resulting in different REE distribution patterns for each sample after normalization to Post-Archean Australian Shale (PAAS, McLennan, 2001). Despite the general progressive enrichment from light (L)REEs to heavy (H)REEs and the pronounced negative Ce anomaly typical for seawater REE patterns, the samples exhibit systematic changes in HREE/LREE ratios (here: $[Yb]_N$ /$[Nd]_N$, whereby "N" refers to PAAS-normalized concentrations). Samples representing NCW have the lowest HREE/LREE ratios near ~3 in contrast to BSAAW samples that reach values of up to 5. Samples representing AW, AW-NCW, NCW, BSAW and PW have intermediate HREE/LREE ratios. As shown in Figure 5b, the increase in HREE/LREE ratios is accompanied by a decrease in $[Nd]_{ID}$. Similarly, the MREE/MREE* ratio (here: $([Gd]_N + [Dy]_N)/([Yb]_N + [Nd]_N)$) and the cerium (Ce) anomaly (i.e. Ce/Ce*, defined as the $[Ce]_N/([[La]_N + [Pr]_N)/2]$) decrease with increasing HREE/LREE (Figs. 5c and d). Only the BSAAW sample with the highest HREE/LREE ratio (station 129, 200 m) has elevated Ce/Ce* (~0.25) compared to what can be expected based on these correlations (~0.05).

The Nd isotopic compositions for all samples range between ε_{Nd} = -14.5 and -8.1 (Figs. 2-4 and 6). The least radiogenic ε_{Nd} signatures were found for samples representing NCW, whereas samples obtained from the core of AW have more radiogenic Nd isotopic compositions with an average ε_{Nd} of -12.4 (1 SD = 0.4, n = 6). Distinctly more radiogenic but also more variable ε_{Nd} signatures were measured in BSAW (average ε_{Nd} = -11.9, 1 SD = 0.2, n = 4), BSAAW (average ε_{Nd} = -9.9, 1 SD = 0.4, n = 2) and PW (average ε_{Nd} = -9.8, 1 SD = 1.3, n = 13) prevailing in the northeastern BS (Figs. 3 and 4). The most radiogenic Nd isotopic compositions are found for PW samples collected about 200 km north of northern Nowaya Zemlya (station 119), where the 100 km wide, cold and less saline body of PW separates BSAW from BSAAW (Fig. 4). In general, the water column in the northeastern BS is marked by constantly decreasing ε_{Nd} signatures with depth reaching values of -12.1 for

bottom waters located in the vicinity of Nowaya Zemlya (station 115, 180 m depth), and -10.2 for bottom water prevailing south of Franz Josef Land (station 126, 350 m depth).

5. DISCUSSION

5.1 Conservative versus non-conservative Nd isotope behavior

The release of REEs from the particulate to the dissolved phase accompanied by a change in the seawater Nd isotope composition is a common feature observed for different marine settings throughout the world's ocean (e.g. Abbott et al., 2015a, b; Grasse et al., 2017; Grenier et al., 2013; Haley et al., 2017; Jeandel, 2016; Lacan and Jeandel, 2005; 2001; Nozaki and Alibo, 2003; Rousseau et al., 2015; Siddall et al., 2008). This process challenges the use of Nd isotopes as a water mass tracer near continental margins because water masses acquire new ε_{Nd} signatures and hence the relationship between ε_{Nd} and hydrographic water mass properties is altered. In the Arctic Mediterranean the release of particulate REEs was suggested to change the dissolved ε_{Nd} signature and [Nd] of Pacific-derived waters entering the AO across the Bering Strait (Charette et al., 2016; Dahlqvist et al., 2007; Porcelli et al., 2009) and to change the Nd characteristics of bottom waters circulating on the North-East Greenland Shelf (Laukert et al., 2017a). In addition, boundary exchange (i.e. modification of ε_{Nd} without significant changes in [Nd]) was suggested to modify the Nd isotope composition of intermediate and deep waters (> ~500 m depth) in the Iceland and Norwegian Seas (Lacan and Jeandel, 2004b; Laukert et al., 2017a). In contrast to these observations, the ε_{Nd} distribution in the upper ~500 m of the open Arctic Mediterranean and on the vast Siberian Arctic shelves was shown to be unaffected by particulate REE release and was interpreted to be mainly the result of lateral advection of water masses and their mixing (Laukert et al., 2017a, b, c).

The observed modification of the Nd isotope composition of intermediate and deep waters in the Arctic Mediterranean is likely caused by interaction between seawater and

young basaltic rocks of Late Neogene and Quaternary age exposed at the margins of the Iceland and Norwegian Seas (cf. Lacan and Jeandel, 2004b). The BS is predominantly surrounded by Caledonian rocks of Ordovician to Early Devonian age and significant changes in the dissolved Nd isotope composition through partial dissolution of deposited sediments are thus less likely. Once the waters with the relatively radiogenic ε_{Nd} signatures (ε_{Nd} ~ -8) resulting from boundary exchange near Iceland are introduced into the large-scale circulation, their signatures are only altered due to water mass mixing but overall well preserved below ~500 m depth throughout the entire Arctic Mediterranean (average ε_{Nd} ~ -10) likely due to the residence time of the REEs exceeding the ventilation time of the intermediate and deep waters (Laukert et al., 2017a). The upper water column (< ~500 m depth) of the Arctic Mediterranean is marked by comparatively low (< ~40 years) ventilation times (Tanhua et al., 2009) and strong lateral advection of water masses in addition to riverine runoff continuously supplying 'new' REEs to the water column, which excludes any significant influence of Icelandic sources on the water column of the shallow BS (average depth ~230 m).

In addition to deep sea boundary exchange, the discharge of large amounts of continental freshwater has been shown to change the dissolved Nd isotope composition through release of river-borne particulate REEs (e.g. Grasse et al., 2017; Rousseau et al., 2015), which was even suggested to be one of the main supply mechanisms of REEs into seawater. The dissolved ε_{Nd} signatures in the BS change towards less radiogenic values along the transport of PW towards the west. This observation would be consistent with the influence of particulate (lithogenic or colloid-bound) Nd from the suspended load of the Yenisei and Ob rivers (dissolved ε_{Nd} of Yenisei and Ob is −5.2 and −6.1, respectively, Zimmermann et al., 2009; riverbed surface sediment ε_{Nd} of Yenisei and Ob on average is −6.4 and −8.2, respectively, Schmitt, 2007) decreasing towards the west. A comparison with shallow Arctic and sub-Arctic shelf regions where changes in the seawater Nd isotope composition and concentration were observed that are beyond what can be expected from water mass

circulation and mixing, provides further insights. Major differences in the REE dynamics observed between these regions (particularly the North-East Greenland Shelf and the Bering and Chukchi Seas) and the release-unaffected Siberian Arctic shelves may be attributed to the different components contained in the dissolved and particulate phases carried by locally supplied freshwaters. Experiments simulating Arctic estuarine mixing recently showed that release of REEs bound to previously coagulated riverine nanoparticles and colloids (NPCs) only occurs when the freshwater end-member is rich in inorganic and poor in organic NPCs (Tepe and Bau, 2016). While this is most likely the case for Greenland-derived freshwater supplied to the North-East Greenland Shelf, the freshwater from the different Siberian rivers in contrast is rich in organic and poor in inorganic NPCs (Dittmar and Kattner, 2003 and references therein). In addition, the content of suspended particulate matter (SPM) transported by the western Siberian rivers including Severnaya Dvina, Yenisei, Ob and Lena is very low (Gordeev, 2006; Gordeev et al., 1996), reducing the potential for dissolution of SPM solid phases (cf. Rousseau et al., 2015). In contrast, the SPM content of the North American rivers (including the Yukon River discharging into the Bering Sea) and that of the Greenland-derived freshwater discharged to the North-East Greenland Shelf is relatively high and hence for these regions SPM dissolution may be another important mechanism changing the dissolved Nd isotope composition. The BS receives comparably little freshwater mostly originating from the Yenisei and Ob rivers and their runoff is both, rich in organic and poor in inorganic NPCs and marked by relatively low SPM concentrations. Based on these considerations it is highly unlikely that the dissolved REE pool in the BS is affected by dissolution of riverine SPM or by remobilization of REEs bound to previously coagulated riverine NPCs.

To support these considerations, we constrain the potential release of Nd from deposited or suspended particles by performing mixing calculations based on salinity, ε_{Nd}, $[Nd]_{ID}$, $\delta^{18}O$ and the end-member values listed in table 3. Note that, despite being considered

individual water masses, the PW and the BS(A)AW are not distinct REE end-member water masses but instead are mixtures between (A)AW and freshwater derived from the open Arctic Mediterranean and the Kara Sea. For simplification we assume that the freshwater is either pure Ob water or a mixture between Ob and Yenisei water. Harms et al. (2000) have shown that extensive mixing between Ob and Yenisei freshwater may occur in the surface layer of the Kara Sea, which is supported by observations from the western Laptev Sea (Laukert et al., 2017b). However, their modeling results also indicate that below the surface layer (> 5 m depth) freshwater from the Ob River may preferentially be advected to the northwestern part of the Kara Sea. Indeed, northward advection of a freshwater component consisting of pure Ob freshwater has recently been confirmed through hydrographic data obtained for the year 2011 (Osadchiev et al., 2017), which justifies our selection of Ob freshwater as the primary riverine end-member. Given that contributions of Yenisei cannot be entirely excluded, we additionally use the Kara Sea freshwater end-member (i.e. mixed freshwater from Ob and Yenisei), which was previously applied by Laukert et al. (2017b) to determine water mass circulation and mixing in the Laptev Sea. In fact, the composition of these rivers likely differs only with regard to their [REE], which in the case of Nd may be more than 10 times higher for the Ob River than for the Yenisei River based on the only available data from two samples (Zimmermann et al., 2009). The riverine end-member Nd isotope signature in our mixing calculation is therefore relatively well constrained while the exact [Nd] value does not affect our conclusions. For all samples and the NCW end-member we also use the initial salinity S_0 instead of the measured salinity S_m to correct for salinity changes related to sea-ice formation or melting. We assume that the ice-related processes do not significantly affect the dissolved Nd isotopic composition (Laukert et al., 2017b).

Essentially all samples plot within the compositional field defined by the three end-members in S-ε_{Nd} space for the case that pure Ob freshwater is used as the freshwater end-member (Fig. 6). In addition, the $\delta^{18}O$-based f_{RF} for each sample is similar to the fraction of

Ob freshwater estimated from the Nd isotope-based mixing calculation. Both observations confirm our considerations that the Ob River must be the main source of freshwater advected to the northeastern Barents Sea. Only the deepest sample of the data set (station 126, 350 m depth) has a f_{RF}, which is too low (0.24 %) compared to the fraction of Ob freshwater (~0.5 %) estimated from the Nd isotope based mixing calculation. However, this sample represents BSAAW, which is formed through transformation (i.e. mostly cooling) of AAW, a process that is not considered in our mixing calculations because AAW is not defined as an end-member. Hence, the compositions of this and the other BSAAW sample by definition cannot be attributed to mixing between the three end-members used. However, the average Nd isotope signature of BSAAW (ε_{Nd} = -9.9, 1 SD = 0.4, n = 2) is identical to that of AAW advected along the Laptev Sea margin (ε_{Nd} = -9.9, 1 SD = 0.2, n = 2; Laukert et al., 2017b), indicating that the Nd isotope composition of the latter is not changed through particulate Nd release during advection into the BS and subsequent transformation to BSAAW. For all other samples the consistency between the $\delta^{18}O$ based f_{RF} and the fraction of Ob freshwater calculated from the Nd isotope based mixing calculations clearly argues against significant release of Nd from particles, which supports our theoretical considerations regarding the dominant control of water mass circulation and mixing on the dissolved Nd isotope distribution in the BS. The release of REEs from other particulate sources is unlikely as well, except for Ce which is found to be elevated in one BSAAW sample (station 129, 200 m depth). The release of particulate Ce is indicated by the deviation of this sample from the negative correlation between Ce/Ce* and HREE/LREE ratios observed for the entire data set (Fig. 5) and attributed to preferential removal of the LREEs over the HREEs from the dissolved phase (section 5.3). In detail, the Ce/Ce* ratio for this sample is too high compared to what can be expected based on this correlation, indicating release of Ce^{3+} from reduced sediments (cf. Haley et al., 2004; Molina-Kescher et al., 2014). Cerium release was also

observed in the Laptev Sea (Laukert et al., 2017b), and likely occurs prior to the release of other REEs when dissolved oxygen falls below a threshold concentration (Haley et al., 2004).

In contrast to our observations, Andersson et al. (2008) suggested that contributions of particulate Nd from Svalbard changed the Nd characteristics of waters circulating in the northwestern BS in 2001. These authors suggested that the [Nd] of the four samples was too high (up to 16.2 pmol/kg) compared to what they had expected from water mass circulation and dilution through sea-ice melt (< ~15 pmol/kg). Our PW sample showing the highest f_{SIM} (~2.7 %) also has a too high $[Nd]_{ID}$ (15.1 pmol/kg) if we consider that addition of sea-ice melt will decrease the [Nd] (Andersson et al., 2008; Laukert et al., 2017b), and if we assume that the [Nd] of AW entering the BS is ~15 pmol/kg (cf. Andersson et al., 2008 and references therein). However, based on our new REE data the average $[Nd]_{ID}$ of AW entering the BS is 16.6 pmol/kg (1 SD = 1.2 pmol/kg), suggesting that the composition of all samples with [Nd] lower than 16.6 pmol/kg can in fact still be entirely attributed to water mass mixing and addition of sea-ice melt whereas contribution of particulate Nd from Svalbard does not have to be considered as an additional Nd source. In fact, the REE concentrations in PW samples that exceed those of AW (e.g. 16.8 pmol/kg for Nd in 2014) may simply reflect the addition of REE-rich Ob freshwater (section 5.2) despite that most of the riverine REEs are removed before the PW reaches the BS (section 5.3).

The absence of significant release of REEs from particles originating from Svalbard to waters circulating in the BS is in line with observations from the western Svalbard Shelf, where waters presumably advected from the BS are also characterized by relatively low [Nd] reaching 14.8 pmol/kg in 2012 (Laukert et al., 2017a). These shelf waters likely have been transported northward within the Sørkapp Current, an extension of the East Spitsbergen Current (Walczowski, 2013 and references therein). Their Nd isotope composition near -11 is similar to that of PW circulating in the northern BS, which not only supports their advection from the BS but also provides further evidence that the BS waters have not been significantly

affected by particulate REE input from Svalbard. In contrast, surface waters north of Svalbard indeed may be affected by inputs of particulate Nd, given that they were characterized by high [Nd] (reaching ~30 pmol/kg) and relatively high salinities in 2001 (Andersson et al., 2008). However, potential seawater-particle interactions north of Svalbard do most likely not affect the dissolved Nd isotope composition in the BS.

5.2 Water mass circulation and mixing in the BS based on Nd isotopes and salinity

We use our data and mixing calculations to refine the understanding of the circulation and mixing of water masses in the BS (cf. Fig. 1). In the central BS, inflowing AW is marked by slightly less radiogenic ε_{Nd} signatures (average ε_{Nd} = -12.4, 1 SD = 0.4, n = 6) compared to AW entering the AO through the Fram Strait (average ε_{Nd} = -11.7, 1 SD = 0.4, n = 11; Laukert et al., 2017a), which implies that the Fram Strait inflow branch is subject to stronger lateral exchange with intermediate waters circulating in the Nordic Seas (average ε_{Nd} = -10.3, 1 SD = 0.9, n = 17; Laukert et al., 2017a) than the BS branch. This is in line with generally lower AW temperatures observed in the Fram Strait, which have been shown to not only result from heat exchange with the atmosphere but also from lateral water mass mixing (Nilsen et al., 2006). In the BS, the least radiogenic signatures are found in the upper ~50 m of the AW core (Fig. 4), providing further evidence that mixing with intermediate waters changes the composition of AW from below (cf. Laukert et al., 2017a). We also observe that the Nd isotope distribution mirrors the salinity distribution within the core of AW whereas the temperature distribution is strongly decoupled (Fig. 4). This indicates that the temperature distribution in the BS indeed is subject to strong air-sea interactions (Yashayaev and Seidov, 2015) and confirms that salinity and Nd isotopes are more suitable to trace water mass circulation and mixing in this region. Decoupling of the temperature can be observed even further south where the core of NCW was present in the upper ~150 m in 2014. Mixing between NCW and AW occurs throughout the entire water column (i.e. down to 250 m depth)

as indicated by the deepest sample of station 42 that has an ε_{Nd} of -13.6±0.4 and therefore is significantly less radiogenic than the average ε_{Nd} of the AW core. Further to the North more radiogenic signatures and lower salinities mark the presence of PW. Even though data from Andersson et al. (2008) were obtained on samples collected in 2001, the ε_{Nd} signatures of these samples agree remarkably well with the signatures expected in this region in 2014 (Fig. 4), suggesting that significant changes in the circulation did not occur in the recent past.

In the northeastern BS, the BS(A)AW bodies are separated by PW with the highest f_{RF} and the most radiogenic Nd isotope compositions (Fig. 4), indicating that most of the Kara Sea freshwater is advected into the BS at ~78 °N. North of this PW front, the Nd isotopic compositions of PW and BSAAW (stations 126 and 129 at 79.5 °N) are more radiogenic compared to those of PW and BSAW circulating near Novaya Zemlya (station 115 at ~73 °N). Based on our mixing calculations this difference results from admixture of small amounts of NCW to the waters circulating south of ~78 °N (i.e. PW and BSAW), even though NCW and PW appear to be separated by AW based on the θ-S (Fig. 2) and $[Nd]_{ID}$ distributions (Fig. 5). However, the separation in θ-S space is mainly attributed to differences in the temperature, which, as mentioned above, is affected by air-sea interactions and hence is actually not suitable to determine water mass circulation and mixing. Similarly, the [Nd] is modified by processes occurring within the water column and hence should not be used to assess the circulation in the BS (section 5.3). Based on our conservative mixing calculations, elevated NCW contributions can also be found in PW samples collected further west (station 99 at 77.7 °N). This supports our observation that part of the NCW is advected away from the coast of Norway and Russia and transported to the northern and northeastern BS mainly by the Novaya Zemlya Current (see Fig. 1). The fraction of NCW transported to the Kara Sea via the Kara Strait (i.e. south of Novaya Zemlya) is unconstrained, but hydrographic observations indicate that the overall volume flux through this passage is ~0.7 Sv (Panteleev et al., 2004). This is significantly lower than the volume flux of NCW that enters the BS via the Norwegian

Coastal Current (~1.8 Sv), supporting our hypothesis that NCW is also advected to the northern BS and eventually leaves the BS to the North or the Northeast.

As mentioned in section 4.1, the different origins of BSAW and BSAAW are only detectable from hydrographic data obtained in 2012 and 2013 further to the east of our eastern section. These data show that relatively warm AAW, which originates from the open AO and which is advected to the Kara Sea via the St. Anna Trough, is transformed into BSAAW before or shortly after entering the BS (Makhotin and Ivanov, 2016). Our deepest samples in the northeastern BS (station 129, 200 m and station 126, 350 m) represent BSAAW and clearly support the open ocean origin of this water mass, given that their Nd isotopic compositions are identical to that of AAW advected along the Laptev margin in the open AO (see also section 5.1). The fate of BSAAW in the northern BS cannot be assessed due to the limited tracer data available from this region, though our data indicate that no BSAAW is present at station 99, which is in line with hydrographic observations (Makhotin and Ivanov, 2016). Most of the BSAAW therefore must be transported either back into the Kara Sea or to the north where it exits the BS through the Franz Victoria Trough (cf. Makhotin and Ivanov, 2016). The Nd isotopic composition of the BSAAW sample collected from the southern end of the Franz Victoria Trough at 200 m depth (station 129) supports this circulation scheme. The BSAW is likely in addition advected to the region west of Franz Josef Land, which can be inferred from hydrographic properties similar to those of inflowing AW and relatively unradiogenic Nd isotope signatures (average ε_{Nd} = -11.8, 1 SD = 0.2, n = 2) encountered in bottom waters at station 99. Advection of AAW from the north was also suggested to occur via the Franz Victoria Trough (Lind and Ingvaldsen, 2012) indicating that complex mixing involving open ocean AAW as well as BSAW and BSAAW must occur in this region. However, based on our limited tracer data this mixing is not unambiguously resolvable and therefore requires dedicated future studies.

5.3 Removal of dissolved REEs during AW transformation

From a geochemical point of view, the most striking feature regarding water mass circulation and mixing in the BS is the removal of dissolved REEs linked to the transformation of (A)AW to BS(A)AW. This process is evident from lower [REE] (reaching only ~11 pmol/kg for $[Nd]_{ID}$) determined for BS(A)AW compared to those determined for (A)AW or PW (Fig. 5). Surprisingly, the BSAW and BSAAW both exhibit the lowest [REE] reported to date for any water mass present in the Arctic Mediterranean. The mixing between (A)AW and PW not only results in a decrease of [Nd] but also causes increasing HREE/LREE and decreasing MREE/MREE* and Ce/Ce* ratios due to stronger removal of the LREEs over the HREEs (Fig. 5). Similar REE dynamics were found in the Laptev Sea where the removal efficiency of dissolved REEs also follows LREEs > MREEs > HREEs and is controlled by estuarine mixing (Laukert et al., 2017b).

To examine REE depletion in the BS, the [Nd] expected prior to REE removal is calculated based on its ε_{Nd} value and the conservative relationship between [Nd] and ε_{Nd} shown in Fig. 6. We assume that the dissolved Nd isotope composition is not affected by particulate REE release (section 5.1) and that the composition of BSAW samples essentially only reflects a mixture between AW and PW. For each sample the calculated [Nd] therefore is the lowest concentration expected prior to REE removal because the unconsidered admixture of NCW would result in even higher [Nd]. Thus, the removal of Nd calculated represents the minimum fraction of Nd removed. Removal for the BSAAW samples is calculated based on the assumption that AAW circulating along the Laptev margin (Laukert et al., 2017b) is the precursor water mass and that the transformation of AAW is mainly driven by cooling (i.e. no significant change in salinity and the Nd isotopic composition is observed). Note that samples representing mixing between AW and NCW (i.e. AW-NCW) do not exhibit depleted $[Nd]_{ID}$ compared to expected [Nd] (Fig. 6), which is why REE removal for these samples is not discussed.

The calculated Nd removal amounts to ~75 % (Fig. 7), which is identical to the removal observed in the Laptev Sea (~75 %, Laukert et al., 2017b) and similar to the mean Nd removal of ~70 % calculated for estuaries globally (Rousseau et al., 2015). The highest removal is determined for the BSAAW samples and for PW samples with the lowest S_0, the highest f_{RF} and the most radiogenic ε_{Nd} signatures. The Nd removal in PW samples is positively correlated with f_{RF} ($R^2 = 0.57$), which contrasts with observations from the Laptev Sea where REE removal is apparently positively correlated with S_0 and negatively with the f_{RF} (Laukert et al., 2017b). However, the samples collected from the Laptev Sea exhibit a wide range of initial salinities including the low-salinity range (~5 < S_0 < ~35), whereas the waters in the BS define a narrower range in S_0 (33.5 < S_0 < 35). On closer examination, a negative correlation between S_0 and Nd removal can also be observed for the marine Laptev Sea samples with S_0 > ~34 (Laukert et al., 2017b). We suggest that the inversion of the relationship between S_0 and Nd removal occurring at S ~34 documents the point where maximum salt-induced estuarine REE removal is reached (for PW circulating in the BS this occurs predominantly in the Ob estuary in the Kara Sea) and any further increase in salinity solely reflects admixture of removal-unaffected marine water masses characterized by high salinities. The observed decrease in the Nd removal in the BS is therefore ultimately a consequence of water mass mixing.

The BSAW samples exhibit REE removal similar to that of PW samples with lowest f_{RF} (for Nd < ~30 %) but compared to the latter plot at slightly lower f_{RF} (Fig. 7). A significantly stronger deviation from the PW trend line is found for the two BSAAW samples. The low [REE] of the BS(A)AW samples thus cannot be related to the estuarine REE removal that occurs in the Kara Sea and instead are likely due to local scavenging by (re)suspended particulate constituents supplied by (A)AW and PW. This is also supported by the HREE/LREE ratio that is highest for the BSAAW samples suggesting that the locally induced REE removal (from 66 to 76 %) results in even stronger preferential LREE depletion than that

occurring during estuarine REE removal in the Kara Sea (Fig. 7). The role of locally formed biogenic particles cannot be directly assessed but a pronounced nutrient depletion is observed at the surface in the formation region of BS(A)AW, which indicates high primary productivity and subsequent lateral transfer of biogenic particles. The latter process thus potentially also contributes to the local REE removal occurring at greater depths. Open ocean removal of REEs through (biogenic) particle scavenging is a common feature observed in all of the world's oceans (e.g. Behrens et al., 2018; Lambelet et al., 2016; Molina-Kescher et al., 2014; Stichel et al., 2012; 2015) and may also generate REE concentrations that fall below those of the REE sources (e.g. Grasse et al., 2017). Our new observations indicate that such processes can occur in semi-enclosed shallow shelf regions such as the BS and may also affect the distribution of other dissolved seawater constituents.

5.4 Implications for the large-scale circulation in the AO based on Nd isotopes

Admixture of dense and cold Kara Sea waters with low [REE] to the AW layer of the open AO was suggested to change the seawater Nd isotope composition towards more radiogenic ε_{Nd} values without significantly changing the [Nd] (Laukert et al., 2017a). In that study the authors argued that the Kara Sea waters would have acquired the ε_{Nd} signature of Yenisei and/or Ob freshwater but at the same time would have low [Nd], since most of the riverine Nd would have been removed from the water column through coagulation of REE-bearing NPCs. Our data from the BS confirm the presence and admixture of such shelf waters, given that Kara Sea sourced PW in the BS on average exhibits more radiogenic Nd isotope compositions (ε_{Nd} = -9.7) than AW entering the AO (ε_{Nd} = -11.7 and -12.4 at Fram Strait and at BS, respectively) but similarly low $[Nd]_{ID}$ ranging between 14.0 and 16.8 pmol/kg. In addition to PW, denser BS(A)AW is also exported through the Kara Sea via the St. Anna Trough, or through the northern BS via the Franz Victoria Trough. These waters also have more radiogenic Nd isotope compositions (average ε_{Nd} = -11.2) and similar $[Nd]_{ID}$ (ranging

between 11.0 and 17.7 pmol/kg) than the inflowing AW indicating that their admixture to the AW layer of the open AO also contributes to the shift towards more radiogenic ε_{Nd} values.

The fate of shallow, freshwater-enriched PW in the open AO is subject of ongoing research. The transport of variable amounts of Siberian freshwater with the Transpolar Drift to the central AO and further to the western Fram Strait was documented by various observational studies (e.g. Alkire et al., 2007; Anderson et al., 2004; Bauch et al., 2011; Jones et al., 2008; Karcher et al., 2006; Rabe et al., 2013; 2009; Taylor et al., 2003). However, the extent of mixing between the distinct Siberian freshwaters could not be conclusively clarified. Recently, Laukert et al. (2017c) suggested that freshwaters from all Arctic rivers are well mixed before being exported via the East Greenland Current through the western Fram Strait. This suggestion is mainly based on a semi-quantitative mixing calculation applied to PW samples from the Fram Strait (Laukert et al., 2017a), and is supported by the observation that extensive mixing between freshwaters supplied by Lena, Yenisei and Ob occurs north of the Laptev Sea (Laukert et al. 2017b). The mixing calculation indicates that the relatively radiogenic Nd isotope composition (ε_{Nd} = -9.9, 1 SD = 0.7, n = 7) of PW that left the AO in summer 2012 may be explained by mixing between AW and Pacific-derived waters and admixture of small amounts of freshwater supplied by all Arctic rivers. However, the possibility that the composition may simply reflect pure mixing between relatively unradiogenic AW and more radiogenic Kara Sea freshwater could not be excluded based on the calculations performed by Laukert et al. (2017a). Our new data from the BS now allow to exclude this scenario, given that mixing between AW and PW in the BS results in similar Nd isotopic compositions but much lower [Nd] (~16 pmol/kg) compared to what has been determined for PW that left the AO across Fram Strait in 2012 (average $[Nd]_{ID}$ = 27.1 pmol/kg, Laukert et al., 2017a). This implies that admixture of Pacific-derived waters with higher [Nd] and of freshwaters from other rivers are necessary to explain the [Nd] of the outflow at Fram Strait, as suggested by Laukert et al. (2017a, c).

6. CONCLUSION

This work presents dissolved neodymium (Nd) isotope compositions, rare earth element (REE) concentrations and stable oxygen isotope compositions obtained on samples collected across the Barents Sea (BS) during summer 2014. The data allow to constrain the transport and transformation of Atlantic Water (AW) in this region and to identify changes in the chemical composition of the water masses beyond what is expected from circulation and mixing alone.

- Similar to observations from the Laptev Sea, no clear evidence is found for the release of REEs from suspended or deposited particles in the BS, which supports the use of Nd isotopes to assess water mass circulation and mixing and to determine the behavior of REEs in this shallow Arctic shelf sea.
- The AW entering the BS through the Nordic Seas dominates the circulation in the BS. Its Nd isotope composition is only slightly less radiogenic (ε_{Nd} = -12.4) than that of AW entering the Arctic Ocean (AO) through the Fram Strait (ε_{Nd} = -11.7) and its core is clearly identifiable by its salinity and the Nd isotope characteristics.
- The core of Norwegian Coastal Water (NCW) is encountered in the southern BS (ε_{Nd} = -14.5) and mixes with AW throughout the entire water column. The admixture of NCW to waters as far north as ~78 °N is clearly indicated by mixing calculations based on Nd isotopes but not discernable in hydrographic properties.
- Barents Sea Atlantic Water (BSAW) and Barents Sea Arctic Atlantic Water (BSAAW) are formed in the northeastern BS through transformation of AW and Arctic Atlantic Water (AAW), respectively. This transformation is mainly driven by heat loss to the atmosphere (in the case of AW) or to the cold Arctic halocline layer (in the case of AAW), but also by admixture of more radiogenic (ε_{Nd} = -9.7) Polar Water (PW) advected mainly from the Kara Sea. The BSAW is transported mainly along the northern coast of Novaya Zemlya via the Novaya Zemlya Current, while the

BSAAW is observed further north and separated from BSAW by a sharp front of PW. The two newly formed water masses cannot be distinguished based on their hydrographic properties in 2014 but differ significantly in their Nd isotope composition due to the different precursor water masses (i.e. AW and AAW) and due to differing admixture of NCW and PW. This results in a less radiogenic Nd isotope signature of BSAW (ε_{Nd} = -11.9) than that of BSAAW (ε_{Nd} = -9.9).

- The transformation of (A)AW to BS(A)AW is accompanied by strong REE removal from the dissolved phase, which occurs in addition to and after salt-induced removal of river-borne REEs in the Kara Sea. The removal observed in BSAW (reaching ~30 %) and BSAAW (reaching ~75 %) is most likely due to scavenging by (re)suspended (biogenic) particles that is not accompanied by subsequent REE release.
- The Nd isotope data from the BS confirm the advection of dense and cold Siberian shelf waters to the open AO. The admixture of BS(A)AW and PW to the AW layer of the open AO contributes to the shift towards more radiogenic Nd isotope signatures observed in the AW layer of the Arctic Mediterranean without significantly changing its REE concentrations.

ACKNOWLEDGEMENTS

We would like to thank the Captain and Crew of the RV Professor Molchanov for help in collecting the seawater samples. We also thank Jutta Heinze (GEOMAR) for laboratory assistance. The expedition to the Barents Sea was funded by the Arctic and Antarctic Research Institute (AARI) within the frame of the project Arctic Floating University 2014 ("Плавучий Университет"). This work is partly based on the Master of Science project of Mariia Petrova and was supported by the joint Russian-German Master Program for Polar and Marine Sciences (POMOR) funded by the German Federal Ministry of Education and Research (BMBF grants 03G0833 and 03F0776), the State University of St. Petersburg and

the Ministry of Education and Science of the Russian Federation. Dorothea Bauch also acknowledges financial support from DFG project BA1689, and Mikhail Makhotin acknowledges financial support from the Ministry of Education and Science of the Russian Federation project RFMEFI61617X0076.

FIGURES AND TABLES

Table 1: Nd isotope, REE concentration and $\delta^{18}O$ data presented in this study along with corresponding hydrographic information. (see attached Excel spreadsheet)

Nr.	SampleID	Cruise	Station	Year	Month	Day	Longitude [°E]	Latitude [°N]	Bot. Depth [m]	CTD Depth [m]	Water Masses	Pressure [db]	σ_ϑ	$\sigma_{0.5}$	Temperature [°C]	pot. T [°C]	CTD Salinity [PSU]	Bottle Salinity [PSU]	Salinity iffi=0 [PSU]	pH	O2 [ml/l]	O2 [%]	Si(OH)4 [µmol/l]	[PO4]3- [µmol/l]	d18O
1	PU14-42-5	PU2014	42	2014	6	7	33.48	71.30	250	5.00	NCW	5.054	27.15	29.44	5.8000	5.79959	34.4466	34.454	34.65	7.957	7.6833	110.4000	0.36	0.487	0.13
2	PU1	PU2	42	201	6	7	33.4	71.	250	100.	NCW	102	27.	29.	4.29	4.2	34.	34.577	34.	7.8	6.7	93.	3.90	0.96	0.1

	4-42-1000	014		4			8	30		99		.094	42	73	1	8324	559		74	39	71	900		3	7
3	PU14-42-160	PU2014	42	2014	6	7	33.48	71.30	250	161.61	AW-NCW	163.406	27.56	29.87	4.673	4.660638	34.7377	34.810	34.93	7.8499	6.7702	93.9900	5.28	1.0633	0.26
4	PU14-42-220	PU2014	42	2014	6	7	33.48	71.30	250	220.84	AW-NCW	223.325	27.63	29.93	4.997	4.997929	34.9962	34.938	35.00	7.8369	6.5779	93.1100	5.40	1.1112	0.29
5	PU14-49-5	PU2014	49	2014	6	8	33.50	73.50	286	5.000	AW-NCW	5.054	27.62	29.92	5.000	4.999961	34.9889	34.936	34.97	8.0066	7.8700	88.2000	0.65	0.5116	0.27
6	PU14-49-5	PU2014	49	2014	6	8	33.50	73.50	286	51.11	AW	51.6733	27.75	30.06	4.472	4.468666	35.0399	35.019	35.01	7.8711	7.0511	98.5000	4.00	1.0822	0.29

	0																							
7	PU14-49-140	PU2014	49	2014	6	8	33.50	73.50	286	141.36	AW	142.937	27.80	30.11	4.092	4.081936	35.046	35.026	35.00	7.8566	7.2100	99.8000	4.841	0.9433	0.28
8	PU14-49-270	PU2014	49	2014	6	8	33.50	73.50	286	266.93	AW	269.996	27.97	30.31	1.9811	1.960604	35.021	34.992	34.99	7.8166	7.2399	95.1000	5.844	0.8944	0.28
9	PU14-54-5	PU2014	54	2014	6	9	33.51	76.00	310	11.035	PW	11.156	27.441	29.78	-0.023	-0.023232	34.1411	34.137	34.99	7.9833	8.5033	105.3000	0.334	0.2888	0.28
10	PU14-54-80	PU2014	54	2014	6	9	33.51	76.00	310	80.71	AW	81.610	27.99	30.33	1.9061	1.901225	35.030	35.009	35.02	7.8911	7.9336	104.1000	1.400	0.6166	0.29
11	PU14-5	PU2014	54	2014	6	9	33.51	76.00	310	151.42	AW	153.13	28.01	30.35	1.7677	1.758704	35.044	35.026	35.07	7.7907	7.6447	99.9000	3.662	1.0033	0.32

	4-150											4				8								
12	PU14-54-285	PU2014	54	2014	6	9	33.51	76.00	310	286.35	AW	289.685	28.09	30.45	0.813	0.79996	35.045	35.040	35.03	7.759	7.172	91.400	6.82	0.934	0.30
13	PU14-99-10	PU2014	99	2014	6	20	46.88	77.68	239	11.48	PW	11.603	27.52	29.90	-0.527	-0.527115	34.253	34.243	34.78	8.078	8.664	105.900	0.65	0.248	0.19
14	PU14-99-60	PU2014	99	2014	6	20	46.88	77.68	239	61.67	PW	62.358	27.90	30.30	-1.701	-1.7001186	34.743	34.662	34.76	7.828	7.861	93.400	1.60	0.834	0.18
15	PU14-99-125	PU2014	99	2014	6	20	46.88	77.68	239	126.49	BSAW	127.925	28.06	30.42	0.585	0.5798	34.943	34.987	34.97	7.825	7.084	89.600	4.08	1.122	0.27
1	P	P	9	2	6	2	4	7	2	1	B	1	2	3	0.	0	3	34	3	7	7	9	4.	0.	0

6	U14-99-180	U2014	9	014		0	6.88	7.68	39	76.14	SAW	78.160	80.5	0.41	348	.340070	4.9860	.952	4.92	.836	.6667	6.500	76	993	.25
17	PU14-1155-10	PU2014	115	2014	6	22	58.51	77.35	206	11.09	PW	11.215	27.72	30.09	0.063	0.062559	34.549	34.527	34.80	8.0144	8.6001	107.100	0.67	0.242	0.220
18	PU14-1155-50	PU2014	115	2014	6	22	58.51	77.35	206	51.39	PW	51.966	27.93	30.32	-1.206	-1.207556	34.7820	34.714	34.87	7.8436	7.4499	90.400	0.89	0.859	0.223
19	PU14-1155-125	PU2014	115	2014	6	22	58.51	77.35	206	126.35	BSAW	127.785	28.03	30.40	0.121	0.116336	34.933	34.918	34.93	7.8177	7.9113	98.900	6.82	0.859	0.25
20	PU14	PU20	115	2014	6	22	58.51	77.3	206	1762	BSAW	178.	28.0	30.4	0.003	-0.0	34.9	34.959	34.9	7.80	7.32	91.4	9.54	0.934	0.27

	-115-180	14						5		7		290	7	4		0376	46		7	5	7	00			
21	PU14-119-10	PU2014	119	2014	6	23	56.41	78.06	177	10.66	PW	10.774	27.61	29.98	-0.280	-0.2800001	34.4000	34.364	34.63	7.892	8.183	100.8000	4.41	0.609	0.12
22	PU14-119-50	PU2014	119	2014	6	23	56.41	78.06	177	51.10	PW	51.667	27.85	30.24	-1.636	-1.6366365	34.6568	34.595	34.69	7.8122	7.8999	94.0000	7.30	0.8599	0.15
23	PU14-119-1000	PU2014	119	2014	6	23	56.41	78.06	177	101.30	PW	102.444	27.91	30.29	-0.847	-0.8495 6	34.7222	34.706	34.71	7.7655	7.3666	89.7000	9.08	0.9177	0.16
24	PU14-1	PU2014	119	2014	6	23	56.41	78.06	177	161.50	PW	163.34	27.97	30.36	-1.135	-1.1395	34.7900	34.767	34.76	7.7600	7.1800	86.7000	9.55	0.9344	0.18

	19-160											4				19								
25	PU14-126-150	PU2014	126	2014	6	23	51.64	79.53	430	151.56	PW	153.298	27.97	30.36	-1.805	-1.808220	34.769	34.734	34.77	7.8066	7.7577	96.2000	5.32	0.8089	0.18
26	PU14-126-355	PU2014	126	2014	6	23	51.64	79.53	430	351.83	BSAAW	356.020	28.07	30.44	-0.146	-0.159571	34.8895	34.944	34.94	7.6588	6.7622	83.3000	16.53	1.0922	0.26
27	PU14-129-10	PU2014	129	2014	6	24	48.58	79.50	310	10.83	PW	10.950	27.74	30.11	-0.043	-0.043091	34.6601	34.545	34.73	7.9889	8.9961	107.9000	0.60	0.217	0.17
28	PU14-12	PU2014	129	2014	6	24	48.58	79.50	310	101.00	PW	102.146	27.93	30.32	-1.204	-1.207070	34.7557	34.714	34.76	7.7935	7.8350	95.0000	3.62	0.734	0.18

	9-1000															4								
29	PU14-1299-1500	PU2014	129	2014	6	24	48.58	79.50	310	151.97	PW	153.715	27.97	30.36	-0.918	-0.922100	34.797	34.782	34.777	7.766	7.725	94.400	6.72	0.809	0.18
30	PU14-1299-2000	PU2014	129	2014	6	24	48.58	79.50	310	201.31	BSAAW	203.636	28.01	30.40	-0.954	-0.960038	34.8330	34.831	34.84	7.6652	7.6066	95.0000	5.49	0.8000	0.21

fswa	fRFa	fSIMa	Nd ID [pmol/kg]	Nd ID rep [pmol/kg]	143/144	Epsilon Nd	143/144 [2sig]	Epsilon Nd [2sig]	Y [pmol/kg]	La [pmol/kg]	Ce [pmol/kg]	Pr [pmol/kg]	Nd [pmol/kg]	Sm [pmol/kg]	Eu [pmol/kg]	Gd [pmol/kg]	Tb [pmol/kg]	Dy [pmol/kg]	Ho [pmol/kg]	Er [pmol/kg]	Tm [pmol/kg]	Yb [pmol/kg]	Lu [pmol/kg]	HREE/LREE[b]	MREE/MREE*[b]	Ce/Ce*[b]
98.	1.0	0.6	22.	22.6	0.5	-14	0.0	0.4	139	30.	17.	5.5	23.	4.1	0.9	5.5	0.8	6.3	1.5	5.1	0.7	4.7	0.8	2.9	1.0	0.3

30	7	3	7		1189 6	.5	0001 8		.0	9	3		0											5	5	0
98.66	0.81	0.52	22.4		0.5111895	-14.5	0.0000018	0.4	1422.0	307.7	15.4	5.4	23.1	4.2	0.9	5.2	0.9	6.2	1.5	5.0	0.7	4.8	0.8	3.000	1.000	0.27
99.35	0.27	0.38	20.2		0.5111933	-13.7	0.0000009	0.2	1322.5	25.6	11.6	4.7	19.8	4.1	0.8	4.8	0.7	5.8	1.5	4.5	0.7	4.6	0.7	3.33	0.99	0.24
99.73	0.08	0.19	21.3		0.5111939	-13.6	0.0000018	0.4	1355.3	26.9	11.9	5.0	21.2	3.9	0.8	5.0	0.9	6.1	1.5	5.1	0.6	4.4	0.7	2.99	1.06	0.24
99.74	0.15	0.111	18.5		0.5111975	-12.9	0.0000010	0.2	1366.4	24.5	11.8	4.6	20.5	4.3	0.8	4.4	0.7	5.5	1.5	4.8	0.7	4.6	0.7	3.27	0.91	0.26
99.99	0.03	-0.02	18.2		0.5111977	-12.9	0.0000009	0.2	1333.5	22.7	9.9	4.3	18.4	3.6	0.8	4.9	0.8	5.3	1.4	4.6	0.6	4.4	0.8	3.46	1.00	0.23
100	0.0	-0.	18.		0.5	-12	0.0	0.3	1311	22.	9.9	4.2	18.	4.4	0.8	4.6	0.7	5.3	1.4	4.8	0.7	4.1	0.7	3.3	1.0	0.2

.02	8	10	0		11986	.7	00014		.4	1			1											0	3	4
99.91	0.10	-0.001	16.1		0.511991	-12.6	0.000022	0.4	128.8	21.5	9.9	3.8	16.8	3.6	0.7	4.8	0.7	5.2	1.4	4.4	0.6	4.6	0.7	3.94	0.97	0.25
97.16	0.15	2.69	15.0		0.5120045	-11.6	0.0000011	0.2	120.6	19.0	8.3	3.1	15.0	3.2	0.6	4.4	0.6	4.7	1.2	4.5	0.5	3.8	0.6	3.68	1.05	0.24
99.95	0.002	0.003	16.3		0.5120016	-12.1	0.0000009	0.2	142.9	22.8	12.3	4.0	17.8	3.9	0.7	4.1	0.8	5.5	1.4	5.0	0.8	3.9	0.8	3.17	1.05	0.29
99.99	-0.13	0.14	16.0		0.5120024	-12.0	0.0000011	0.2	124.9	18.9	9.2	3.4	16.0	2.9	0.7	4.1	0.7	4.8	1.4	4.5	0.6	4.2	0.7	3.82	0.93	0.26
100.05	-0.001	-0.004	15.1		0.5120111	-12.2	0.0000011	0.2	130.1	20.5	11.0	3.7	15.5	3.6	0.7	4.0	0.6	5.0	1.3	4.3	0.6	4.2	0.7	3.92	0.95	0.29
97.	0.7	1.6	14.		0.5	-10	0.0	0.3	124	18.	6.6	3.3	14.	2.9	0.6	4.1	0.7	5.1	1.2	4.3	0.6	3.7	0.7	3.7	1.0	0.1

58	3	9	0		120779	.9	000013		.6	6			3											7	9	9
98.93	0.76	0.31	14.6	14.2	0.5120092	-10.6	0.0000012	0.2	125.0	18.1	6.8	3.0	13.3	2.9	0.7	4.0	0.7	4.6	1.2	4.1	0.6	3.8	0.7	4.111	1.02	0.21
99.90	0.14	-0.04	14.1		0.5120039	-11.7	0.0000013	0.3	129.8	19.7	6.1	3.3	15.2	3.4	0.7	3.8	0.7	4.9	1.4	4.7	0.6	4.3	0.7	4.06	0.91	0.17
99.81	0.29	-0.10	17.7	18.3	0.5120023	-12.0	0.0000013	0.3	128.2	19.9	7.9	3.1	15.3	3.1	0.7	4.0	0.6	4.8	1.4	4.3	0.6	4.3	0.7	4.07	0.91	0.23
98.48	0.66	0.85	15.1		0.5120036	-11.7	0.0000013	0.3	130.4	20.9	8.4	3.6	16.2	3.6	0.6	4.6	0.7	5.3	1.3	4.5	0.7	4.2	0.7	3.74	1.03	0.22
99.06	0.46	0.48	15.9		0.5120035	-11.8	0.0000017	0.3	130.6	19.4	8.1	3.5	15.2	3.4	0.7	4.3	0.7	5.0	1.3	4.4	0.6	4.5	0.8	4.26	0.94	0.23
99.	0.2	0.0	13.		0.5	-11	0.0	0.3	130	19.	6.5	3.2	14.	3.1	0.8	4.7	0.7	5.1	1.2	4.5	0.6	4.1	0.7	4.0	1.0	0.1

69	8	3	1		12035	.8	000013		.2	3			4											8	8	9
99.81	0.16	0.03	15.3		0.5120019	-12.1	0.000013	0.3	129.1	20.9	10.0	3.5	15.3	3.7	0.9	4.5	0.6	4.8	1.3	4.6	0.7	4.2	0.6	3.94	0.99	0.27
98.02	1.13	0.85	16.8		0.5122203	-8.5	0.000015	0.3	137.9	20.0	8.8	3.5	17.0	3.8	0.9	5.1	0.8	5.7	1.5	5.0	0.7	4.8	0.8	4.04	1.01	0.24
98.74	0.97	0.29	16.3		0.5122222	-8.1	0.000013	0.3	134.6	18.2	6.0	3.3	15.1	3.5	0.9	4.8	0.8	5.7	1.4	5.2	0.7	4.8	0.8	4.60	0.99	0.18
99.09	0.89	0.02	15.6		0.5122205	-8.5	0.000013	0.3	141.1	18.5	6.1	3.3	16.8	3.5	0.9	4.0	0.8	5.9	1.5	5.5	0.7	5.1	0.7	4.37	0.89	0.18
99.27	0.74	-0.01	15.0		0.5121169	-9.2	0.000013	0.3	141.1	19.1	4.8	3.5	16.4	3.6	0.8	4.5	0.8	5.5	1.5	5.0	0.7	4.8	0.8	4.24	0.94	0.14
99.	0.7	0.1	14.		0.5	-9.	0.0	0.3	125	17.	5.7	3.2	15.	3.2	0.7	4.4	0.6	5.1	1.4	4.6	0.6	4.3	0.7	4.1	0.9	0.1

16	4	0	3		121666	2	000013		.1	9			2											2	8	7
99.77	0.24	-0.001	11.0		0.5121118	-10.2	0.0000013	0.3	112.9	14.5	2.0	2.3	11.3	2.0	0.6	3.3	0.5	3.9	1.1	4.0	0.6	3.8	0.6	4.84	0.87	0.08
98.56	0.84	0.60	15.4		0.5121172	-9.1	0.0000020	0.4	139.0	19.8	7.2	3.5	16.8	4.1	0.9	4.5	0.8	6.3	1.5	5.1	0.7	4.6	0.7	3.92	1.04	0.20
99.10	0.76	0.15	14.9		0.5121178	-9.0	0.0000013	0.3	138.8	18.3	5.5	3.4	15.5	3.6	0.7	4.5	0.7	5.8	1.5	4.7	0.7	4.7	0.7	4.35	0.99	0.16
99.31	0.72	-0.03	14.4		0.5121559	-9.3	0.0000014	0.3	139.2	18.2	5.6	3.3	15.2	3.3	0.8	4.6	0.7	5.3	1.4	4.7	0.6	4.3	0.8	4.06	1.04	0.17
99.45	0.53	0.02	12.7		0.5121147	-9.6	0.0000011	0.2	124.6	16.8	7.2	2.7	12.9	2.8	0.7	3.5	0.6	4.7	1.2	4.5	0.6	4.6	0.7	5.09	0.84	0.24

Table 2: Water masses and their characteristics in the Barents Sea in 2014. Uncertainties are provided as 1 SD in brackets.

Water masses	n[a]	σ_θ	S[b]	θ	ε_{Nd}	$[Nd]_{ID}$ pmol/kg[c]	HREE/LREE[d]	MREE/MREE*[d]	Ce/Ce*[d]
NCW - Norwegian Coastal Water (S < 34.7; θ > 2 °C)	2	27.28 (0.19)	34.52 (0.09)	5.04 (1.07)	-14.5 (0.0)	22.5 (0.3)	3.0 (0.0)	1.0 (0.0)	0.3 (0.0)
AW - Atlantic-derived Water (S > 35; θ > 0 °C; 27.70 < σ_θ ≤ 28.09)	6	27.93 (0.13)	35.02 (0.02)	2.50 (1.45)	-12.4 (0.4)	16.6 (1.2)	3.6 (0.3)	1.0 (0.0)	0.3 (0.0)
PW - Arctic-derived Polar Water (S < 34.8; θ < 0 °C)	13	27.80 (0.19)	34.58 (0.21)	-0.87 (0.66)	-9.8 (1.3)	15.2 (0.8)	4.1 (0.3)	1.0 (0.1)	0.2 (0.0)
BSAW - Barents Sea Atlantic Water (34.8 < S < 35.0; θ < 2 °C; σ_θ > 27.8)	4	28.05 (0.02)	34.95 (0.03)	0.26 (0.26)	-11.9 (0.2)	15.0 (2.0)	4.0 (0.1)	1.0 (0.1)	0.2 (0.0)
BSAAW - Barents Sea Arctic Atlantic Water (34.8 < S < 35.0; θ < 2 °C; σ_θ > 27.8)	2	28.04 (0.04)	34.89 (0.08)	-0.56 (0.57)	-9.9 (0.4)	11.8 (1.2)	5.0 (0.2)	0.9 (0.0)	0.2 (0.1)

[a] Number of measurements.

[b] Bottle salinity

[c] Determined via the isotope dilution method.

[d] Normalized to PAAS (McLennan, 2001).

Table 3: End-member compositions used in this study.

Table 3: End-member compositions of the REE sources applied in this study.

REE sources	S	ε_{Nd}	[Nd]	water types[a]	$\delta^{18}O$
NCW - Norwegian Coastal Water	34.70[b]	-14.5[c]	22.5[c]		-
AW - Atlantic-derived Water	35.02[c]	-12.4[c]	16.6[c]	SW	0.3[c]
KS - Kara Sea freshwater (Ob and Yenisei)	0	-6.0[d]	963[d]	RF	-15.5[f]
Ob freshwater	0	-6.1[e]	2152[e]	RF	-15.5[f]
Sea ice	4[g]	-	-	SIM	-2[g]

[a] Water types defined for the mass balance calculation based on S and $\delta^{18}O$.

[b] Average of the initial salinity S_0 of NCW samples.

[c] Average of samples from this study.

[d] Values taken from Laukert et al. (2017b)

[e] Values taken from Zimmermann et al. (2009).

[f] Values taken from Dubinina et al. (2017).

[g] Values taken from Bauch and Cherniavskaia (2018) and references therein.

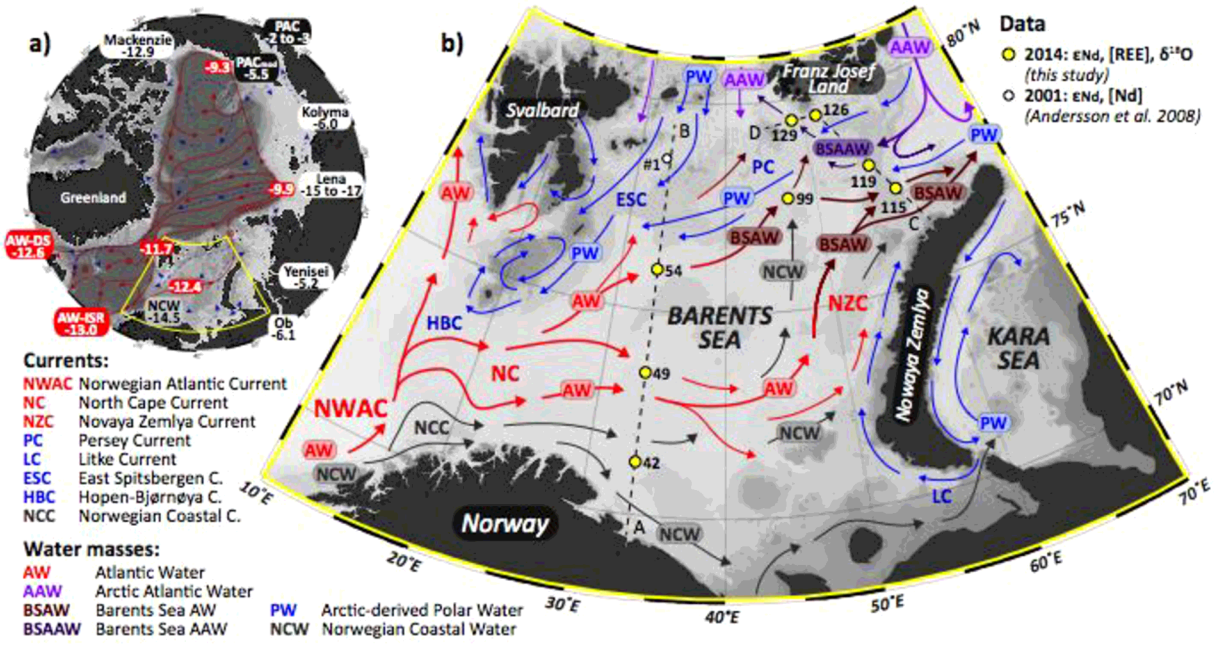

Figure 1: a) Bathymetric map (IBCAO, Jakobsson et al., 2012) of the Arctic Mediterranean (i.e. AO and Nordic Seas) with circulation scheme of the upper layers (dashed blue lines) and subsurface Atlantic and intermediate layers (solid red lines) (modified after Rudels et al., 2012). The REE sources with known ε_{Nd} signatures and [Nd] are Atlantic-derived Water (AW) advected through the Iceland–Scotland Ridge (AW-ISR) and the Denmark Strait (AW-DS), Norwegian Coastal Water (NCW), Pacific-derived Water (PAC), modified Pacific-derived Water (PACmod) and the major Arctic rivers Ob, Yenisei, Lena, Kolyma and Mackenzie (Charette et al., 2016; Dahlqvist et al., 2007; Lacan and Jeandel, 2004a, b; Laukert et al., 2017a, b; Persson et al., 2011; Porcelli et al., 2009; Zimmermann et al., 2009). The change in the Nd isotopic composition within the AW layer is shown at key sites. Circled crosses indicate sites of convection or sinking from intermediate and AW layers to deeper levels. The area shown in b) is highlighted in yellow. b) Barents Sea region with locations of the water samples obtained in 2014 (this study) and 2001 (Andersson et al., 2008) shown together with their station numbers. Information on the classification of the water masses is given in the main text. The circulation scheme shown here was adopted from Loeng (1991) and Pfirman et al. (1994) but further refined according to observations made here and in other

studies focusing on the hydrography of the BS (Harris et al., 1998; Lien and Trofimov, 2013; Makhotin and Ivanov, 2016; Oziel et al., 2016). Figures were produced using Ocean Data View (Schlitzer, 2018) and modified manually.

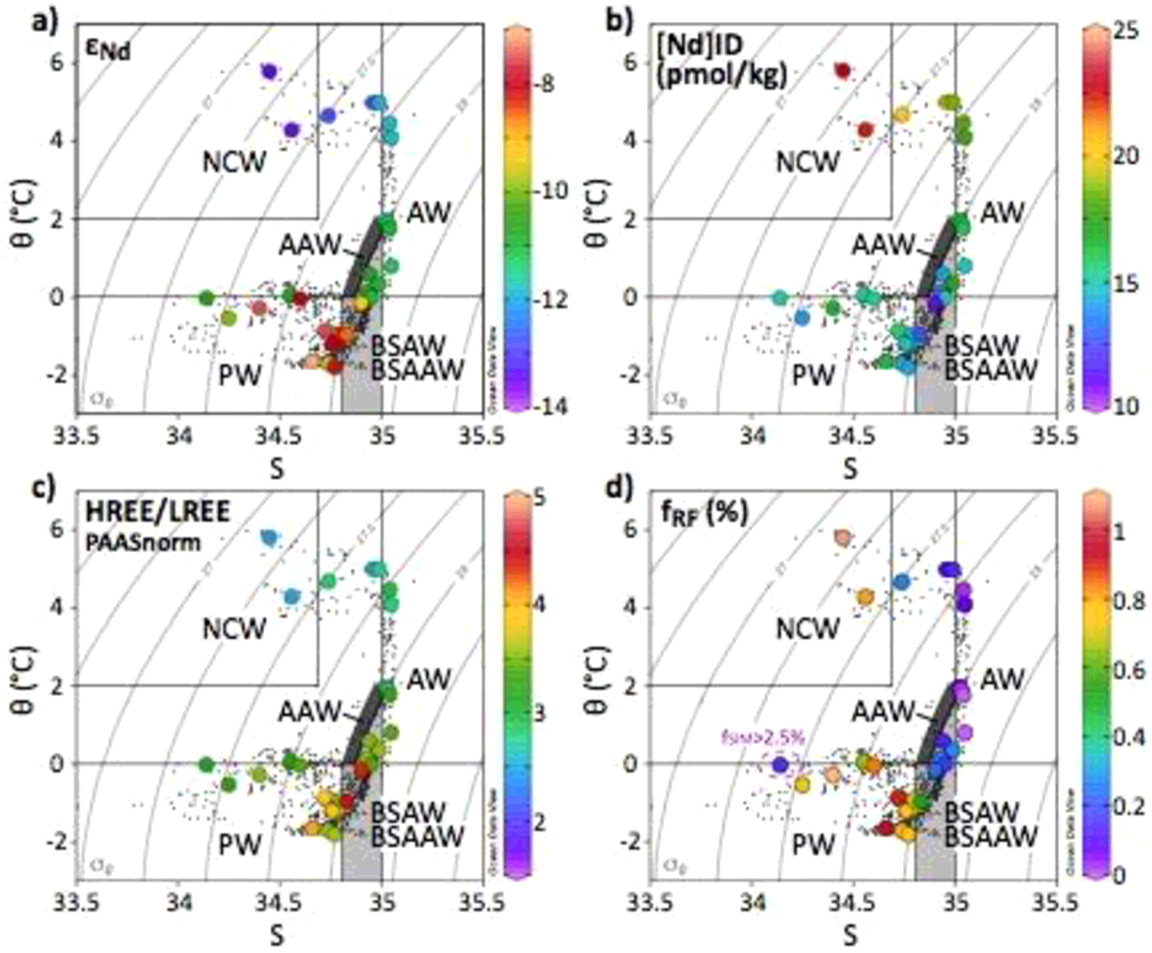

Figure 2: Potential temperature versus salinity plots with potential density isopycnals, together with a) ε_{Nd} values, b) Nd concentrations determined via isotope dilution ($[Nd]_{ID}$), c) PAAS-normalized HREE/LREE ratios and d) fractions of riverine freshwater (f_{RF}) shown as color-coded circles. In addition, all CTD data are shown from the 2014 cruise (Makhotin and Ivanov, 2016). Water masses are classified based on the basis of constant θ-S end-member definitions (after Rudels et al., 2012; 2005) and observations made in this study and by Makhotin and Ivanov (2016) and Oziel et al. (2016). Water masses are labeled as follows: Norwegian Coastal Water – NCW, Polar Water – PW, Atlantic Water - AW, Arctic Atlantic

Water – AAW, Barents Sea Atlantic Water – BSAW and Barents Sea Arctic Atlantic Water – BSAAW. Note that BSAW and BSAAW cannot be distinguished based on the hydrographic data from 2014 alone. Plots produced using Ocean Data View (Schlitzer, 2018) and modified manually.

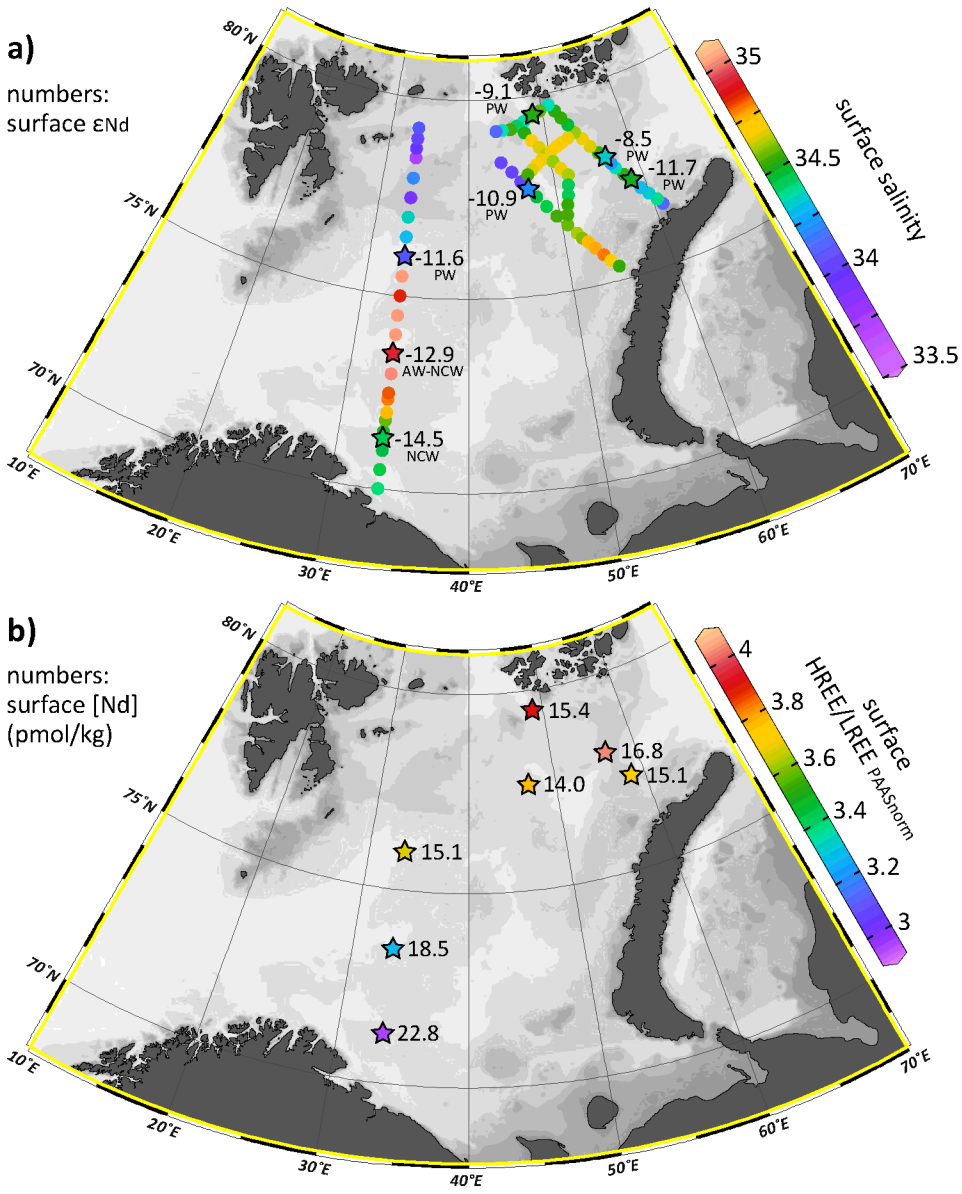

Figure 3: Surface distribution of a) ε_{Nd} data together with sample salinities (color-coded stars) and CTD salinity for 2014 (Makhotin and Ivanov, 2016), and b) Nd concentrations determined via isotope dilution ($[Nd]_{ID}$) and the PAAS-normalized HREE/LREE ratios

(color-coded stars). Figures were produced using Ocean Data View (Schlitzer, 2018) and modified manually.

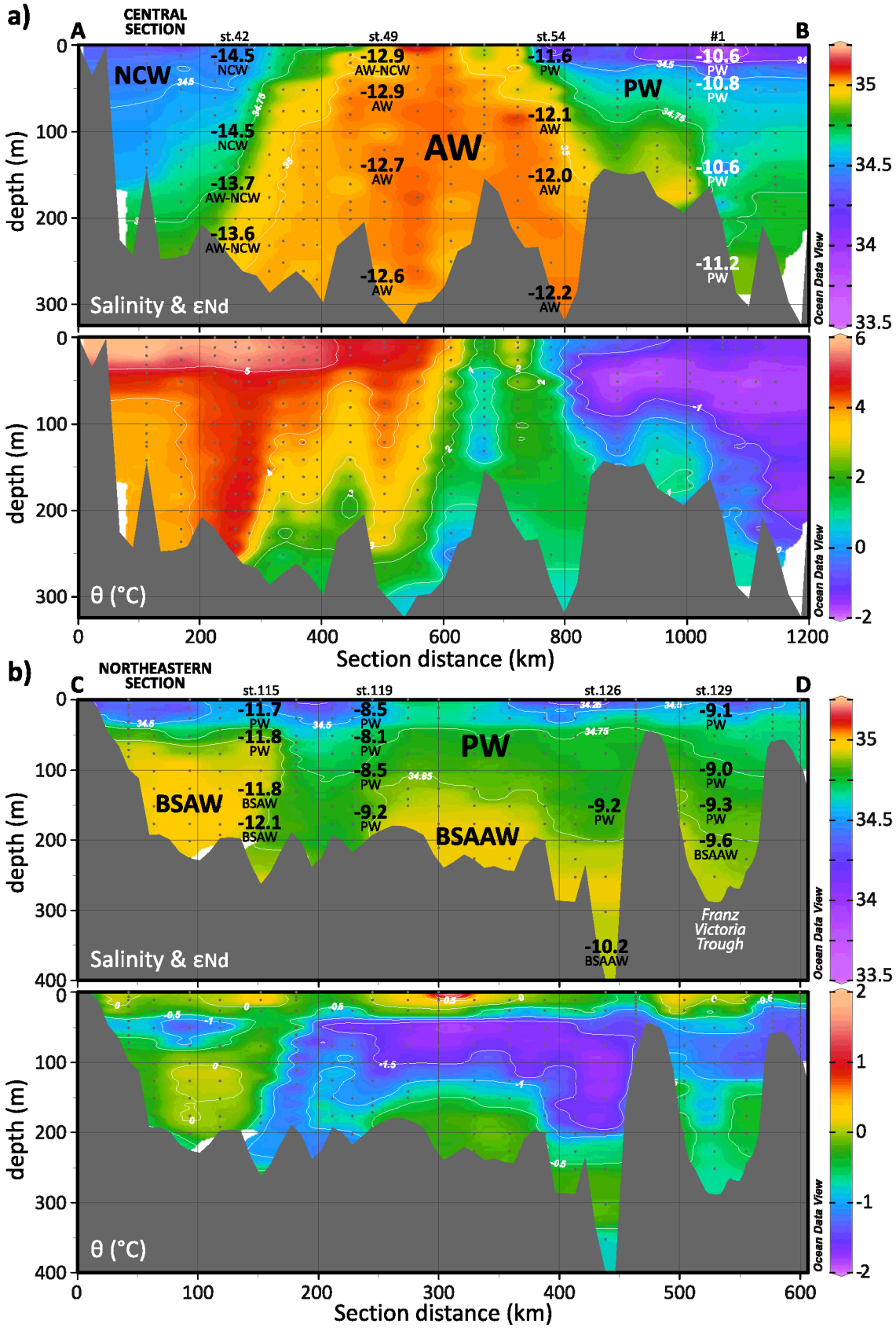

Figure 4: Distribution of the salinity and the potential temperature (all CTD data, Makhotin and Ivanov, 2016) along the longitudinal sections in a) the central Barents Sea (section A-B)

and b) the northeastern Barents Sea (section C-D) with the Nd isotopic composition shown as numbers in the salinity sections. The distribution of water masses as defined in the main text and in Fig. 2 is indicated in addition. The numbers of the stations where Nd isotope samples were taken are given above the sections. Station #1 (white numbers) is from Andersson et al. (2008). Sections were produced using Ocean Data View (Schlitzer, 2018) and modified manually.

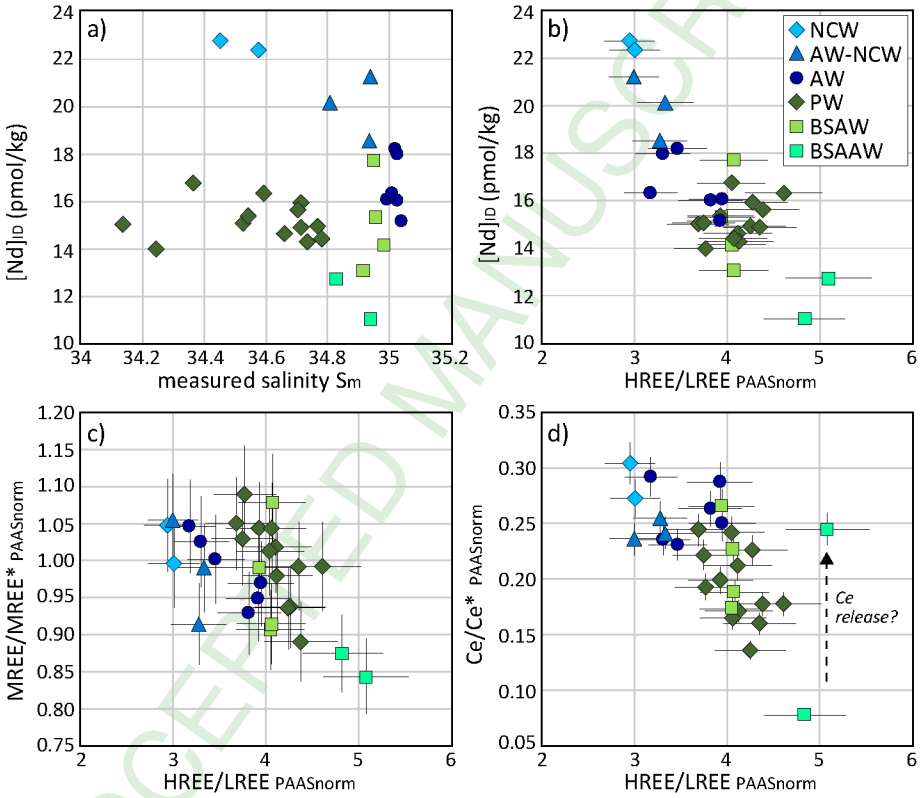

Figure 5: a) Nd concentration determined via isotope dilution ($[Nd]_{ID}$) versus measured salinity S_m, and the PAAS normalized HREE/LREE ratio against b) $[Nd]_{ID}$, c) the PAAS normalized MREE/MREE* ratio and d) the PAAS normalized Ce/Ce* ratio. Error bars represent the external 2-sigma error for repeat measurements of calibration standards (see main text for further information).

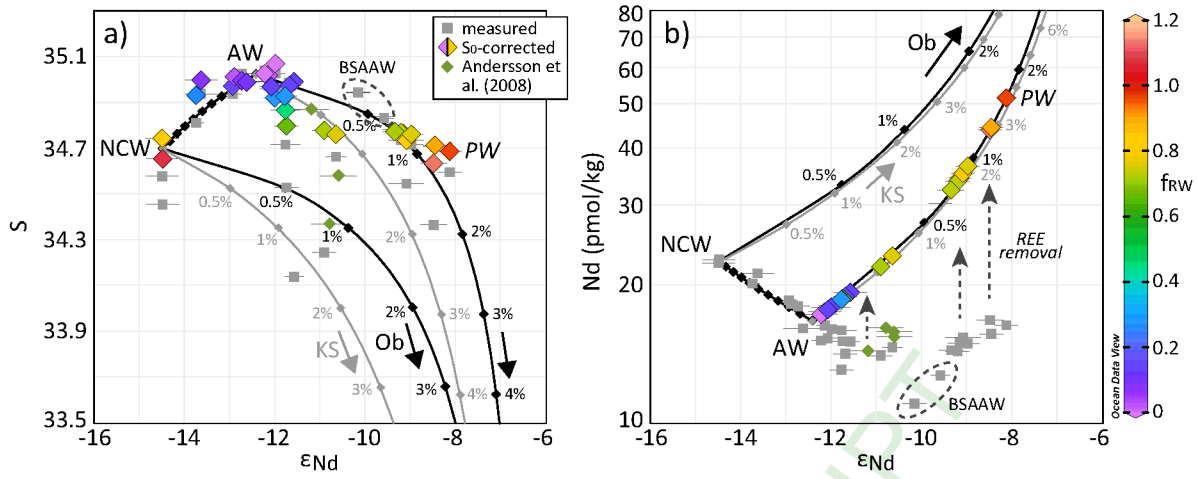

Figure 6: a) Salinity versus ε_{Nd}, and b) [Nd] versus ε_{Nd}. The end-member (table 2) mixing lines are shown between Norwegian Coastal Warter (NCW), Atlantic-derived Water (AW) and Kara Sea freshwater (KS, grey mixing lines) and Ob freshwater (Ob, black mixing lines). Note that Polar Water (PW) is not a distinct REE source but instead a mixture of AW and Ob freshwater. The measured data are given by the grey symbols, while the color-coded symbols represent data with the initial salinity S_0 instead of the measured salinity S_m, and with corrected [Nd] determined with the conservative end-member mixing calculation (i.e. based on ε_{Nd} and the initial salinity S_0). The correction was not performed for the two samples representing BSAAW, given that this water mass is transformed AAW that was not considered in our mixing calculations. Error bars represent the external 2-sigma error.

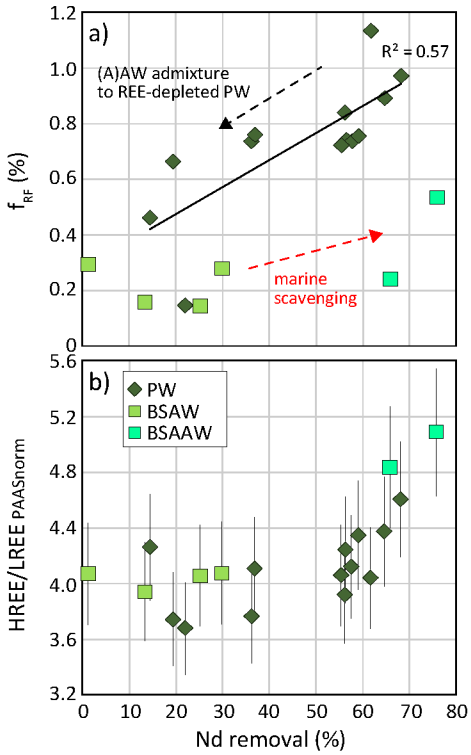

Figure 7: Calculated Nd removal versus a) f_{RF}, and b) the PAAS normalized HREE/LREE ratios.

REFERENCES

Abbott, A.N., Haley, B.A., McManus, J., 2015a. Bottoms up: Sedimentary control of the deep North Pacific Ocean's εNd signature. Geology, 43(11): 1035-1035. http://dx.doi.org/10.1130/g37114.1.

Abbott, A. N., Haley, B. A., McManus, J., Reimers, C. E., 2015b. The sedimentary flux of dissolved rare earth elements to the ocean. Geochim. Cosmochim. Acta, 154: 186-200. http://dx.doi.org/10.1016/j.gca.2015.01.010.

Alkire, M. B., Falkner, K. K., Rigor, I., Steele, M., Morison, J., 2007. The return of Pacific waters to the upper layers of the central Arctic Ocean. Deep-Sea Res. Pt I, 54(9): 1509-1529. http://dx.doi.org/10.1016/j.dsr.2007.06.004.

Anderson, L. G., Jutterstrom, S., Kaltin, S., Jones, E. P., Bjork, G. R., 2004. Variability in river runoff distribution in the Eurasian Basin of the Arctic Ocean. J. Geophys. Res. Oceans, 109(C1). http://dx.doi.org/10.1029/2003jc001773.

Andersson, P. S., Porcelli, D., Frank, M., Bjork, G., Dahlqvist, R., Gustafsson, O., 2008. Neodymium isotopes in seawater from the Barents Sea and Fram Strait Arctic-Atlantic gateways. Geochim. Cosmochim. Acta, 72(12): 2854-2867. http://dx.doi.org/10.1016/j.gca.2008.04.008.

Ardyna, M., Babin, M., Gosselin, M., Devred, E., Bélanger, S., Matsuoka, A., Tremblay, J. É, 2013. Parameterization of vertical chlorophyll a in the Arctic Ocean: impact of the subsurface chlorophyll maximum on regional, seasonal, and annual primary production estimates. Biogeosciences, 10(6): 4383-4404. http://dx.doi.org/10.5194/bg-10-4383-2013.

Arrigo, K. R., van Dijken, G. L., 2015. Continued increases in Arctic Ocean primary production. Prog. Oceanogr., 136: 60-70. http://dx.doi.org/10.1016/j.pocean.2015.05.002.

Arsouze, T., Dutay, J. C., Lacan, F., Jeandel, C., 2009. Reconstructing the Nd oceanic cycle using a coupled dynamical - biogeochemical model. Biogeosciences, 6(12): 2829-2846. http://dx.doi.org/10.5194/bg-6-2829-2009.

Årthun, M., Eldevik, T., Smedsrud, L. H., Skagseth, Ø., Ingvaldsen, R. B., 2012. Quantifying the Influence of Atlantic Heat on Barents Sea Ice Variability and Retreat. J. Climate, 25(13): 4736-4743. http://dx.doi.org/10.1175/jcli-d-11-00466.1.

Barrat, J. A., Keller, F., Amosse, J., Taylor, R. N., Nesbitt, R. W., Hirata, T., 1996. Determination of rare earth elements in sixteen silicate reference samples by ICP-MS after Tm addition and ion exchange separation. Geostandard Newslett., 20(1): 133-139. http://dx.doi.org/10.1111/j.1751-908X.1996.tb00177.x.

Bauch, D., Cherniavskaia, E., 2018. Water Mass Classification on a Highly Variable Arctic Shelf Region: Origin of Laptev Sea Water Masses and Implications for the Nutrient Budget. J. Geophys. Res. Oceans, 123(3): 1896-1906. http://dx.doi.org/10.1002/2017jc013524.

Bauch, D., Rudgers van der Loeff, M., Andersen, N., Torres-Valdes, S., Bakker, K., Abrahamsen, E. P., 2011. Origin of freshwater and polynya water in the Arctic Ocean halocline in summer 2007. Prog. Oceanogr., 91(4): 482-495. http://dx.doi.org/10.1016/j.pocean.2011.07.017.

Behrens, M. K., Pahnke, K., Paffrath, R., Schnetger, B., Brumsack, H.-J., 2018. Rare earth element distributions in the West Pacific: Trace element sources and conservative vs. non-conservative behavior. Earth Planet Sci. Lett., 486: 166-177. http://dx.doi.org/10.1016/j.epsl.2018.01.016.

Björk, G., Gustafsson, B. G., Stigebrandt, A., 2001. Upper layer circulation of the Nordic seas as inferred from the spatial distribution of heat and freshwater content and potential energy. Polar Res., 20(2): 161-168. http://dx.doi.org/10.1111/j.1751-8369.2001.tb00052.x.

Charette, M. A., Lam, P. J., Lohan, M. C., Kwon, E. Y., Hatje, V., Jeandel, C., Shiller, A. M., Cutter, G. A., Thomas, A., Boyd, P. W., Homoky, W. B., Milne, A., Thomas, H., Andersson, P. S., Porcelli, D., Tanaka, T., Geibert, W., Dehairs, F., Garcia-Orellana, J., 2016. Coastal ocean and shelf-sea biogeochemical cycling of trace elements and isotopes: lessons learned from GEOTRACES. Philos. Trans. A Math. Phys. Eng. Sci., 374(2081): Artn 20160076. http://dx.doi.org/10.1098/rsta.2016.0076.

Craig, H., 1961. Isotopic Variations in Meteoric Waters. Science, 133(3465): 1702-3. http://dx.doi.org/10.1126/science.133.3465.1702.

Dahlqvist, R., Andersson, P. S., Porcelli, D., 2007. Nd isotopes in Bering Strait and Chukchi Sea Water. Geochim. Cosmochim. Acta, 71: A196.

Dittmar, T., Kattner, G., 2003. The biogeochemistry of the river and shelf ecosystem of the Arctic Ocean: a review. Mar. Chem., 83(3-4): 103-120. http://dx.doi.org/10.1016/S0304-4203(03)00105-1.

Dmitrenko, I. A., Bauch, D., Kirillov, S. A., Koldunov, N., Minnett, P. J., Ivanov, V. V., Hölemann, J. A., Timokhov, L. A., 2009. Barents Sea upstream events impact the properties of Atlantic water inflow into the Arctic Ocean: Evidence from 2005 to 2006 downstream observations. Deep Sea Res. Pt I, 56(4): 513-527. http://dx.doi.org/10.1016/j.dsr.2008.11.005.

Dubinina, E. O., Kossova, S. A., Miroshnikov, A. Y., Fyaizullina, R. V., 2017. Isotope parameters (δD, δ18O) and sources of freshwater input to Kara Sea. Oceanology, 57(1): 31-40. http://dx.doi.org/10.1134/s0001437017010040.

Epstein, S., Mayeda, T., 1953. Variation of O18 content of waters from natural sources. 4(5): 213-224. http://dx.doi.org/10.1016/0016-7037(53)90051-9.

Eriksen, E., Skjoldal, H. R., Gjøsæter, H., Primicerio, R., 2017. Spatial and temporal changes in the Barents Sea pelagic compartment during the recent warming. Prog. Oceanogr., 151: 206-226. http://dx.doi.org/10.1016/j.pocean.2016.12.009.

Frank, M., 2002. Radiogenic isotopes: Tracers of past ocean circulation and erosional input. Rev. Geophys., 40(1): 1001. http://dx.doi.org/10.1029/2000rg000094.

Gascard, J.-C., 2004. The Norwegian Atlantic Current in the Lofoten basin inferred from hydrological and tracer data (129I) and its interaction with the Norwegian Coastal Current. Geophys. Res. Lett., 31(1). http://dx.doi.org/10.1029/2003gl018303.

Goldstein, S. L., Hemming, S. R., 2003. Long-lived Isotopic Tracers in Oceanography, Paleoceanography, and Ice-sheet Dynamics. In: Elderfield, H., Holland, H. D., Turekian, K. K. (Eds.), Treatise on Geochemistry. Elsevier, pp. 625.

Gordeev, V. V., 2006. Fluvial sediment flux to the Arctic Ocean. Geomorphology, 80(1-2): 94-104. http://dx.doi.org/10.1016/j.geomorph.2005.09.008.

Gordeev, V. V., Martin, J. M., Sidorov, I. S., Sidorova, M. V., 1996. A reassessment of the Eurasian river input of water, sediment, major elements, and nutrients to the Arctic Ocean. Am. J. Sci., 296(6): 664-691. http://dx.doi.org/10.2475/ajs.296.6.664.

Grasse, P., Bosse, L., Hathorne, E. C., Böning, P., Pahnke, K., Frank, M., 2017. Short-term variability of dissolved rare earth elements and neodymium isotopes in the entire water column of the Panama Basin. Earth Planet Sci. Lett. http://dx.doi.org/10.1016/j.epsl.2017.07.022.

Grasshoff, K., Kremling, K., Ehrhardt, M., 2009. Methods of seawater analysis. John Wiley & Sons, http://dx.doi.org/10.1002/9783527613984.

Grenier, M., Jeandel, C., Lacan, F., Vance, D., Venchiarutti, C., Cros, A., Cravatte, S., 2013. From the subtropics to the central equatorial Pacific Ocean: Neodymium isotopic composition and rare earth element concentration variations. J. Geophys. Res. Oceans, 118(2): 592-618. http://dx.doi.org/10.1029/2012jc008239.

Haley, B. A., Du, J., Abbott, A. N., McManus, J., 2017. The Impact of Benthic Processes on Rare Earth Element and Neodymium Isotope Distributions in the Oceans. Front. Mar. Sci., 4. http://dx.doi.org/10.3389/fmars.2017.00426.

Haley, B. A., Klinkhammer, G. P., McManus, J., 2004. Rare earth elements in pore waters of marine sediments. Geochim. Cosmochim. Acta, 68(6): 1265-1279. http://dx.doi.org/10.1016/j.gca.2003.09.012.

Harms, I. H., Karcher, M. J., Dethleff, D., 2000. Modelling Siberian river runoff - implications for contaminant transport in the Arctic Ocean. J. Mar. Syst., 27(1-3): 95-115. http://dx.doi.org/10.1016/S0924-7963(00)00062-2.

Harris, C. L., Plueddemann, A. J., Gawarkiewicz, G. G., 1998. Water mass distribution and polar front structure in the western Barents Sea. J. Geophys. Res. Oceans, 103(C2): 2905-2917. http://dx.doi.org/10.1029/97jc02790.

Hathorne, E. C., Haley, B. A., Stichel, T., Grasse, P., Zieringer, M., Frank, M., 2012. Online preconcentration ICP-MS analysis of rare earth elements in seawater. Geochem. Geophy. Geosy., 13(1): Artn Q01020. http://dx.doi.org/10.1029/2011gc003907.

Ingvaldsen, R. B., Asplin, L., Loeng, H., 2004. Velocity field of the western entrance to the Barents Sea. J. Geophys. Res. Oceans, 109(C3). http://dx.doi.org/10.1029/2003jc001811.

Jakobsson, M., Mayer, L., Coakley, B., Dowdeswell, J. A., Forbes, S., Fridman, B., Hodnesdal, H., Noormets, R., Pedersen, R., Rebesco, M., Schenke, H. W., Zarayskaya, Y., Accettella, D., Armstrong, A., Anderson, R. M., Bienhoff, P., Camerlenghi, A., Church, I., Edwards, M., Gardner, J. V., Hall, J. K., Hell, B., Hestvik, O., Kristoffersen, Y., Marcussen, C., Mohammad, R., Mosher, D., Nghiem, S. V., Pedrosa, M. T., Travaglini, P. G., Weatherall, P., 2012. The International Bathymetric Chart of the Arctic Ocean (IBCAO) Version 3.0. Geophys. Res. Lett., 39(12): Artn L12609. http://dx.doi.org/10.1029/2012gl052219.

Jacobsen, S.B., Wasserburg, G.J., 1980. Sm-Nd Isotopic Evolution of Chondrites. Earth and Planetary Science Letters 50, 139-155. http://dx.doi.org/10.1016/0012-821x(80)90125-9.

Jeandel, C., 2016. Overview of the mechanisms that could explain the 'Boundary Exchange' at the land-ocean contact. Philos. Trans. A Math. Phys. Eng. Sci., 374(2081): Artn 20150287. http://dx.doi.org/10.1098/rsta.2015.0287.

Johannesson, K.H., Burdige, D.J., 2007. Balancing the global oceanic neodymium budget: Evaluating the role of groundwater. Earth Planet. Sci. Lett., 253(1-2): 129-142. http://dx.doi.org/10.1016/j.epsl.2006.10.021.

Johannesson, K.H. Chevis, D. A., Burdige, D. J., Cable, J. E., Martin, J. B., Roy, M., 2011. Submarine groundwater discharge is an important net source of light and middle REEs to coastal waters of the Indian River Lagoon, Florida, USA. Geochim. Cosmochim. Acta, 75(3): 825-843. http://dx.doi.org/10.1016/j.gca.2010.11.005.

Johannesson, K.H., Palmore, C. D., Fackrell, J., Prouty, N. G., Swarzenski, P. W., Chevis, D., Telfeyan, K., White, C. D., Burdige, D. J., 2017. Rare earth element behavior during groundwater–seawater mixing along the Kona Coast of Hawaii. Geochim. Cosmochim. Acta, 198: 229-258. http://dx.doi.org/10.1016/j.gca.2016.11.009.

Jones, E. P., Anderson, L. G., Jutterstrom, S., Mintrop, L., Swift, J. H., 2008. Pacific freshwater, river water and sea ice meltwater across Arctic Ocean basins: Results from the 2005 Beringia Expedition. J. Geophys. Res. Oceans, 113(C8): Artn C08012. http://dx.doi.org/10.1029/2007jc004124.

Karcher, M., Gerdes, R., Kauker, F., 2006. Modeling of δ18O and 99Tc dispersion in Arctic and subarctic seas. ASOF Newlsetter.

Korablev, A., Smirnov, A., Baranova, O. K., 2014. Climatological Atlas of the Nordic Seas and Northern North Atlantic. NOAA Atlas NESDIS 77.

Lacan, F., Jeandel, C., 2001. Tracing Papua New Guinea imprint on the central Equatorial Pacific Ocean using neodymium isotopic compositions and Rare Earth Element patterns. Earth Planet. Sci. Lett., 186(3-4): 497-512. http://dx.doi.org/10.1016/S0012-821x(01)00263-1.

Lacan, F., Jeandel, C., 2004a. Denmark Strait water circulation traced by heterogeneity in neodymium isotopic compositions. Deep-Sea Res. Pt I, 51(1): 71-82. http://dx.doi.org/10.1016/j.dsr.2003.09.006.

Lacan, F., Jeandel, C., 2004b. Neodymium isotopic composition and rare earth element concentrations in the deep and intermediate Nordic Seas: Constraints on the Iceland Scotland Overflow Water signature. Geochem. Geophy. Geosy., 5(11): Artn Q11006. http://dx.doi.org/10.1029/2004gc000742.

Lacan, F., Jeandel, C., 2005. Neodymium isotopes as a new tool for quantifying exchange fluxes at the continent-ocean interface. Earth Planet. Sci. Lett., 232(3-4): 245-257. http://dx.doi.org/10.1016/j.epsl.2005.01.004.

Lambelet, M., van de Flierdt, T., Crocket, K., Rehkamper, M., Kreissig, K., Coles, B., Rijkenberg, M. J. A., Gerringa, L. J. A., de Baar, H. J. W., Steinfeldt, R., 2016. Neodymium isotopic composition and concentration in the western North Atlantic Ocean: Results from the GEOTRACES GA02 section. Geochim. Cosmochim. Acta, 177: 1-29. http://dx.doi.org/10.1016/j.gca.2015.12.019.

Laukert, G., Frank, M., Bauch, D., Hathorne, E. C., Rabe, B., von Appen, W.-J., Wegner, C., Zieringer, M., Kassens, H., 2017a. Ocean circulation and freshwater pathways in the Arctic Mediterranean based on a combined Nd isotope, REE and oxygen isotope section across Fram Strait. Geochim. Cosmochim. Acta, 202: 285-309. http://dx.doi.org/10.1016/j.gca.2016.12.028.

Laukert, G., Frank, M., Bauch, D., Hathorne, E. C., Gutjahr, M., Janout, M., Hölemann, J., 2017b. Transport and transformation of riverine neodymium isotope and rare earth element signatures in high latitude estuaries: A case study from the Laptev Sea. Earth Planet. Sci. Lett., 477: 205-217. http://dx.doi.org/10.1016/j.epsl.2017.08.010.

Laukert, G., Frank, M., Hathorne, E. C., Krumpen, T., Rabe, B., Bauch, D., Werner, K., Peeken, I., Kassens, K., 2017c. Pathways of Siberian freshwater and sea ice in the

Arctic Ocean traced with radiogenic neodymium isotopes and rare earth elements. Polarforschung, 87: 3-13. http://dx.doi.org/10.2312/polarforschung.87.1.3.

Le Fèvre, B., Pin, C., 2005. A straightforward separation scheme for concomitant Lu–Hf and Sm–Nd isotope ratio and isotope dilution analysis. Anal. Chim. Acta., 543(1-2): 209-221. http://dx.doi.org/10.1016/j.aca.2005.04.044.

Levitus, S., Matishov, G., Seidov, D., Smolyar, I., 2009. Barents Sea multidecadal variability. Geophys. Res. Lett., 36(19). http://dx.doi.org/10.1029/2009gl039847.

Lien, V. S., Trofimov, A. G., 2013. Formation of Barents Sea Branch Water in the north-eastern Barents Sea. Pol. Res., 32(1). http://dx.doi.org/10.3402/polar.v32i0.18905.

Lind, S., Ingvaldsen, R. B., 2012. Variability and impacts of Atlantic Water entering the Barents Sea from the north. 62: 70-88. http://dx.doi.org/10.1016/j.dsr.2011.12.007.

Lind, S., Ingvaldsen, R. B., Furevik, T., 2016. Arctic layer salinity controls heat loss from deep Atlantic layer in seasonally ice-covered areas of the Barents Sea. Geophys. Res. Lett., 43(10): 5233-5242. http://dx.doi.org/10.1002/2016gl068421.

Loeng, H., 1991. Features of the Physical Oceanographic Conditions of the Barents Sea. Polar Res., 10(1): 5-18. http://dx.doi.org/10.1111/j.1751-8369.1991.tb00630.x.

Makhotin, M. S., Ivanov, V. V., 2016. Circulation of the Atlantic water in the Barents Sea based on hydrological survey data and numerical simulation. Proc. Hydrometcentre of Russia, 361: 169-191.

Mauritzen, C., Hansen, E., Andersson, M., Berx, B., Beszczynska-Möller, A., Burud, I., Christensen, K. H., Debernard, J., de Steur, L., Dodd, P., Gerland, S., Godøy, Ø, Hansen, B., Hudson, S., Høydalsvik, F., Ingvaldsen, R., Isachsen, P. E., Kasajima, Y., Koszalka, I., Kovacs, K. M., Køltzow, M., LaCasce, J., Lee, C. M., Lavergne, T., Lydersen, C., Nicolaus, M., Nilsen, F., Nøst, O. A., Orvik, K. A., Reigstad, M., Schyberg, H., Seuthe, L., Skagseth, Ø, Skarðhamar, J., Skogseth, R., Sperrevik, A., Svensen, C., Søiland, H., Teigen, S. H., Tverberg, V., Wexels Riser, C., 2011. Closing

the loop – Approaches to monitoring the state of the Arctic Mediterranean during the International Polar Year 2007–2008. Prog. Oceanogr., 90(1-4): 62-89. http://dx.doi.org/10.1016/j.pocean.2011.02.010.

McLennan, S. M., 2001. Relationships between the trace element composition of sedimentary rocks and upper continental crust. Geochem. Geophy. Geosy., 2(4): n/a-n/a. http://dx.doi.org/10.1029/2000gc000109.

Molina-Kescher, M., Frank, M., Hathorne, E.C., 2014. South Pacific dissolved Nd isotope compositions and rare earth element distributions: Water mass mixing versus biogeochemical cycling. Geochim. Cosmochim. Acta, 127: 171-189. http://dx.doi.org/10.1016/j.gca.2013.11.038.

Molina-Kescher, M., Hathorne, E. C., Osborne, A. H., Behrens, M. K., Kölling, M., Pahnke, Frank, M., 2018. The Influence of Basaltic Islands on the Oceanic REE Distribution: A Case Study From the Tropical South Pacific. Front. Mar. Sci., 5. http://dx.doi.org/10.3389/fmars.2018.00050.

Morrison, R., Waldner, A., Hathorne, E. C., Rahlf, P., Zieringer, M, Montagna, P., Colin, C., Frank, N., Frank, M., submitted. Limited influence of basalt weathering inputs on the seawater neodymium isotope composition of the northern Iceland Basin. Chem. Geol.

Nilsen, F., Gjevik, B., Schauer, U., 2006. Cooling of the West Spitsbergen Current: Isopycnal diffusion by topographic vorticity waves. J. Geophys. Res. Oceans, 111(C8). http://dx.doi.org/10.1029/2005jc002991.

Nozaki, Y., Alibo, D. S., 2003. Importance of vertical geochemical processes in controlling the oceanic profiles of dissolved rare earth elements in the northeastern Indian Ocean. Earth Planet. Sci. Lett., 205(3-4): 155-172. http://dx.doi.org/10.1016/s0012-821x(02)01027-0.

Onarheim, I.H., Eldevik, T., Smedsrud, L.H., Stroeve, J.C., 2018. Seasonal and Regional Manifestation of Arctic Sea Ice Loss. J. Climate, 31(12): 4917-4932. http://dx.doi.org/10.1175/jcli-d-17-0427.1.

Osadchiev, A.A., Izhitskiy, A.S., Zavialov, P.O., Kremenetskiy, V.V., Polukhin, A.A., Pelevin, V.V., Toktamysova, Z.M., 2017. Structure of the buoyant plume formed by Ob and Yenisei river discharge in the southern part of the Kara Sea during summer and autumn. J. Geophys. Res. Oceans, 122(7): 5916-5935. http://dx.doi.org/10.1002/2016jc012603.

Osborne, A. H., Haley, B.A., Hathorne, E. C., Plancherel, Y., Frank, M., 2015. Rare earth element distribution in Caribbean seawater: Continental inputs versus lateral transport of distinct REE compositions in subsurface water masses. Mar. Chem., 177: 172-183. http://dx.doi.org/10.1016/j.marchem.2015.03.013.

Östlund, H. G., Hut, G., 1984. Arctic Ocean water mass balance from isotope data. J. Geophys. Res., 89(C4). http://dx.doi.org/10.1029/JC089iC04p06373.

Oziel, L., Neukermans, G., Ardyna, M., Lancelot, C., Tison, J. L., Wassmann, P., Sirven, J., Ruiz-Pino, D., Gascard, J. C., 2017. Role for Atlantic inflows and sea ice loss on shifting phytoplankton blooms in the Barents Sea. J. Geophys. Res. Oceans, 122(6): 5121-5139. http://dx.doi.org/10.1002/2016jc012582.

Oziel, L., Sirven, J., Gascard, J. C., 2016. The Barents Sea frontal zones and water masses variability (1980-2011). Ocean Sci., 12(1): 169-184. http://dx.doi.org/10.5194/os-12-169-2016.

Panteleev, G., Ikeda, M., Grotov, A., Nechaev, D., Yaremchuk, M., 2004. Mass, Heat and Salt Balances in the Eastern Barents Sea Obtained by Inversion of Hydrographic Section Data. Journal of Oceanography, 60(3): 613-623. http://dx.doi.org/10.1023/B:JOCE.0000038353.37993.e1.

Persson, P. O., Andersson, P. S., Porcelli, D., Semiletov, I. P., 2011. The influence of Lena River water inflow and shelf sediment-sea water exchange for the Nd isotopic composition in the Laptev Sea and Arctic Ocean. Geophys. Res. Abstr., 13.

Pfirman, S. L., Bauch, D., Gammelsrød, T., 1994. The Northern Barents Sea: Water Mass Distribution and Modification, The Polar Oceans and Their Role in Shaping the Global Environment. Geophysical Monograph Series, pp. 77-94.

Pin, C., Zalduegui, J. F. S., 1997. Sequential separation of light rare-earth elements, thorium and uranium by miniaturized extraction chromatography: Application to isotopic analyses of silicate rocks. Analyt. Chim. Acta, 339(1-2): 79-89. http://dx.doi.org/10.1016/s0003-2670(96)00499-0.

Polyakov, I. V., Pnyushkov, A. V., Alkire, M. B., Ashik, I. M., Baumann, T. M., Carmack, E., Goszczko, I., , Guthrie, J., Ivanov, V. V., Kanzow, T., Krishfield, R., Kwok, R., Sundfjord, A., Morison, J., Rember, R., Yulin, A., 2017. Greater role for Atlantic inflows on sea-ice loss in the Eurasian Basin of the Arctic Ocean. Science, 356(6335): 285-291. http://dx.doi.org/10.1126/science.aai8204.

Porcelli, D., Andersson, P. S., Baskaran, M., Frank, M., Bjork, G., Semiletov, I. (2009. The distribution of neodymium isotopes in Arctic Ocean basins. Geochim. Cosmochim. Acta, 73(9): 2645-2659. http://dx.doi.org/10.1016/j.gca.2008.11.046.

Proshutinsky, A. Y., Johnson, M. A., 1997. Two circulation regimes of the wind-driven Arctic Ocean. J. Geophys. Res. Oceans, 102(C6): 12493-12514. http://dx.doi.org/10.1029/97jc00738.

Rabe, B., Dodd, P. A., Hansen, E., Falck, E., Schauer, U., Mackensen, A., Beszczynska-Möller, A., Kattner, G., Rohling, E. J., Cox, K., 2013. Liquid export of Arctic freshwater components through the Fram Strait 1998-2011. Ocean Sci., 9(1): 91-109. http://dx.doi.org/10.5194/os-9-91-2013.

Rabe, B., Schauer, U., Mackensen, A., Karcher, M., Hansen, E., Beszczynska-Möller, A., 2009. Freshwater components and transports in the Fram Strait - recent observations and changes since the late 1990s. Ocean Sci., 5(3): 219-233. http://dx.doi.org/10.5194/os-5-219-2009.

Rempfer, J., Stocker, T. F., Joos, F., Dutay, J. C., Siddall, M., 2011. Modelling Nd-isotopes with a coarse resolution ocean circulation model: Sensitivities to model parameters and source/sink distributions. Geochim. Cosmochim. Acta, 75(20): 5927-5950. http://dx.doi.org/10.1016/j.gca.2011.07.044.

Rickli, J., Frank, M., Halliday, A. N., 2009. The hafnium-neodymium isotopic composition of Atlantic seawater. Earth Planet. Sci. Lett., 280(1-4): 118-127. http://dx.doi.org/10.1016/j.epsl.2009.01.026.

Rousseau, T. C., Sonke, J. E., Chmeleff, J., van Beek, P., Souhaut, M., Boaventura, G., Seyler, P., Jeandel, C., 2015. Rapid neodymium release to marine waters from lithogenic sediments in the Amazon estuary. Nat. Commun., 6: 7592. http://dx.doi.org/10.1038/ncomms8592.

Rudels, B., 2012. Arctic Ocean circulation and variability - advection and external forcing encounter constraints and local processes. Ocean Sci., 8(2): 261-286. http://dx.doi.org/10.5194/os-8-261-2012.

Rudels, B., Bjork, G., Nilsson, J., Winsor, P., Lake, I., Nohr, C., 2005. The interaction between waters from the Arctic Ocean and the Nordic Seas north of Fram Strait and along the East Greenland Current: results from the Arctic Ocean-02 Oden expedition. J. Mar. Syst., 55(1-2): 1-30. http://dx.doi.org/10.1016/j.jmarsys.2004.06.008.

Sakshaug, E., 2004. Primary and secondary production in the Arctic Seas. In: Stein, R., Macdonald, R. (Eds.), The Organic Carbon Cycle in the Arctic Ocean. Springer, Berlin, pp. 57-81.

Schlitzer, R., 2018. Ocean Data View.

Schmitt, W., 2007. Application of the Sm–Nd Isotope System to the Late Quaternary Paleoceanography of the Yermak Plateau. (Arctic Ocean). Dissertation. Fakultät für Geowissenschaften. Ludwig-Maximilians-Universität München (LMU).

Seidov, D., Antonov, J. I., Arzayus, K. M., Baranova, O. K., Biddle, M., Boyer, T. P., Johnson, D. R., Mishonov, A. V., Paver, C., Zweng, M. M., 2015. Oceanography north of 60 degrees N from World Ocean Database. Prog. Oceanogr., 132: 153-173. http://dx.doi.org/10.1016/j.pocean.2014.02.003.

Siddall, M., Khatiwala, S., van de Flierdt, T., Jones, K., Goldstein, S. L., Hemming, S., Anderson, R. F., 2008. Towards explaining the Nd paradox using reversible scavenging in an ocean general circulation model. Earth Planet. Sci. Lett., 274(3-4): 448-461. http://dx.doi.org/10.1016/j.epsl.2008.07.044.

Skagseth, Ø., 2008. Recirculation of Atlantic Water in the western Barents Sea. Geophys. Res. Lett., 35(11). http://dx.doi.org/10.1029/2008gl033785.

Skagseth, O., Drinkwater, K. F., Terrile, E., 2011. Wind- and buoyancy-induced transport of the Norwegian Coastal Current in the Barents Sea. J. Geophys. Res. Oceans, 116(C8). http://dx.doi.org/10.1029/2011jc006996.

Stichel, T., Frank, M., Rickli, J., Haley, B. A., 2012. The hafnium and neodymium isotope composition of seawater in the Atlantic sector of the Southern Ocean. Earth Planet. Sci. Lett., 317: 282-294. http://dx.doi.org/10.1016/j.epsl.2011.11.025.

Stichel, T., Hartman, A. E., Duggan, B., Goldstein, S. L., Scher, H., Pahnke, K., 2015. Separating biogeochemical cycling of neodymium from water mass mixing in the Eastern North Atlantic. Earth Planet. Sci. Lett., 412: 245-260. http://dx.doi.org/10.1016/j.epsl.2014.12.008.

Tachikawa, K., Athias, V., Jeandel, C., 2003. Neodymium budget in the modern ocean and paleo-oceanographic implications. J. Geophys. Res. Oceans, 108(C8). http://dx.doi.org/10.1029/1999jc000285.

Tanaka, T., Togashi, S., Kamioka, H., Amakawa, H., Kagami, H., Hamamoto, T., Yuhara, M., Orihashi, Y., Yoneda, S., Shimizu, H., Kunimaru, T., Takahashi, K., Yanagi, T., Nakano, T., Fujimaki, H., Shinjo, R., Asahara, Y., Tanimizu, M., Dragusanu, C., 2000. JNdi-1: a neodymium isotopic reference in consistency with LaJolla neodymium. Chem. Geol., 168(3-4): 279-281. http://dx.doi.org/10.1016/s0009-2541(00)00198-4.

Tanhua, T., Jones, E. P., Jeansson, E., Jutterström, S., Smethie, W. M., Wallace, D. W. R., Anderson, L. G., 2009. Ventilation of the Arctic Ocean: Mean ages and inventories of anthropogenic CO2and CFC-11. J. Geophys. Res., 114(C1). http://dx.doi.org/10.1029/2008jc004868.

Taylor, J. R., Falkner, K. K., Schauer, U., Meredith, M., 2003. Quantitative considerations of dissolved barium as a tracer in the Arctic Ocean. J. Geophys. Res. Oceans, 108(C12). http://dx.doi.org/10.1029/2002jc001635.

Tepe, N., Bau, M., 2016. Behavior of rare earth elements and yttrium during simulation of arctic estuarine mixing between glacial-fed river waters and seawater and the impact of inorganic (nano-)particles. Chem. Geol., 438: 134-145. http://dx.doi.org/10.1016/j.chemgeo.2016.06.001.

van de Flierdt, T., Pahnke, K., Amakawa, H., Andersson, P. S., Basak, C., Coles, B., Colin, C., Crocket, K., Frank, M., Frank, N., Goldstein, S. L., Goswami, V., Haley, B. A., Hathorne, E. C., Hemming, S. R., Henderson, G. M., Jeandel, C., Jones, K., Kreissig, K., Lacan, F., Lambelet, M., Martin, E. E., Newkirk, D. R., Obata, H., Pena, L., Piotrowski, A. M., Pradoux, C., Scher, H. D., Schöberg, H., Singh, S. K., Stichel, T., Tazoe, H., Vance, D., Yang, J., 2012. GEOTRACES intercalibration of neodymium isotopes and rare earth element concentrations in seawater and suspended particles. Part 1: reproducibility of results for the international intercomparison. Limnol. Oceanogr. Methods, 10(4): 234-251. http://dx.doi.org/10.4319/lom.2012.10.234.

Walczowski, W., 2013. Frontal structures in the West Spitsbergen Current margins. Ocean Sci., 9(6): 957-975. http://dx.doi.org/10.5194/os-9-957-2013.

Yashayaev, I., Seidov, D., 2015. The role of the Atlantic Water in multidecadal ocean variability in the Nordic and Barents Seas. Prog. Oceanogr., 132: 68-127. http://dx.doi.org/10.1016/j.pocean.2014.11.009.

Zimmermann, B., Porcelli, D., Frank, M., Andersson, P. S., Baskaran, M., Lee, D. C., Halliday, A. N., 2009. Hafnium isotopes in Arctic Ocean water. Geochim. Cosmochim. Acta, 73(11): 3218-3233. http://dx.doi.org/10.1016/j.gca.2009.02.028.

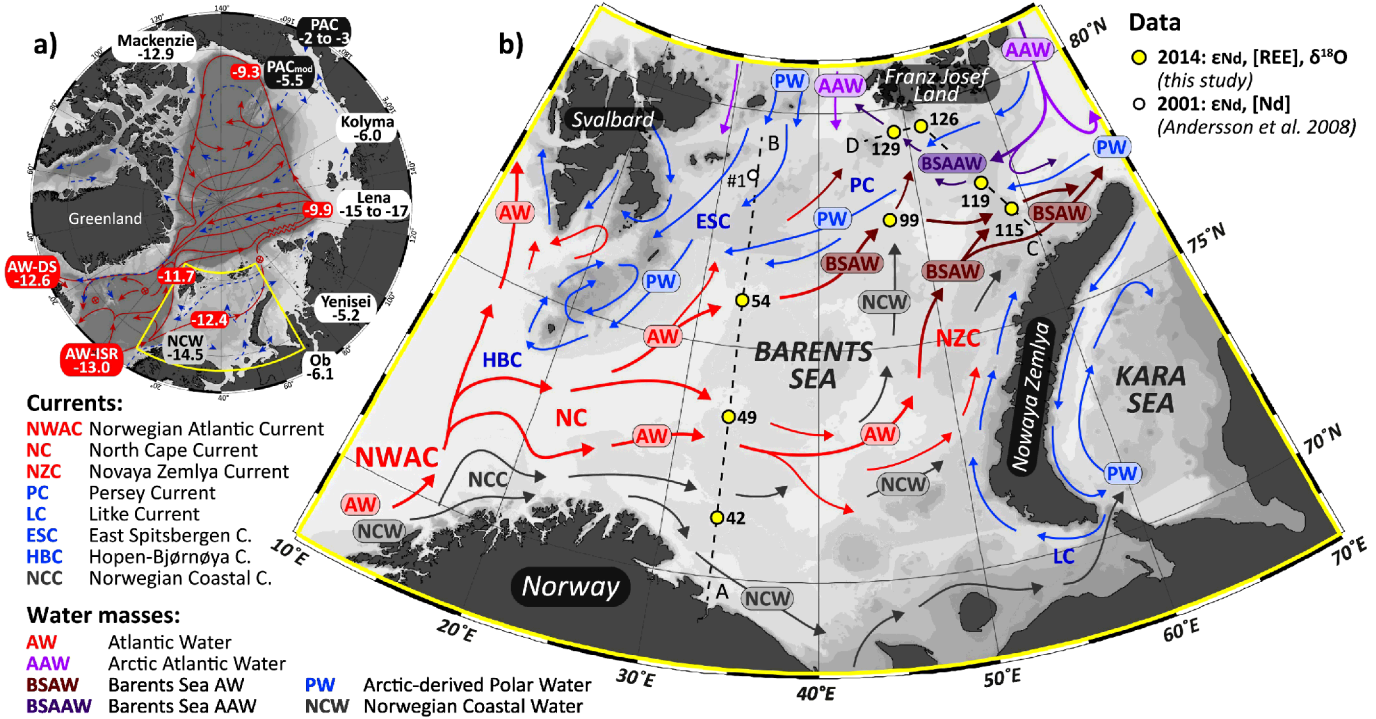
a)
Mackenzie -12.9
PAC -2 to -3
PAC$_{mod}$ -5.5
-9.3
Kolyma -6.0
Greenland
Lena -15 to -17
-9.9
AW-DS -12.6
-11.7
Yenisei -5.2
-12.4
NCW -14.5
AW-ISR -13.0
Ob -6.1
b)
Svalbard
Franz Josef Land
Nowaya Zemlya
BARENTS SEA
KARA SEA
Norway
80°N
75°N
70°N
10°E
20°E
30°E
40°E
50°E
60°E
70°E
Data
2014: εNd, [REE], δ18O
(this study)
2001: εNd, [Nd]
(Andersson et al. 2008)
Currents:
NWAC Norwegian Atlantic Current
NC North Cape Current
NZC Novaya Zemlya Current
PC Persey Current
LC Litke Current
ESC East Spitsbergen C.
HBC Hopen-Bjørnøya C.
NCC Norwegian Coastal C.
Water masses:
AW Atlantic Water
AAW Arctic Atlantic Water
BSAW Barents Sea AW
BSAAW Barents Sea AAW
PW Arctic-derived Polar Water
NCW Norwegian Coastal Water
#1
A
B
C
D
126
129
119
115
99
54
49
42

Figure 1

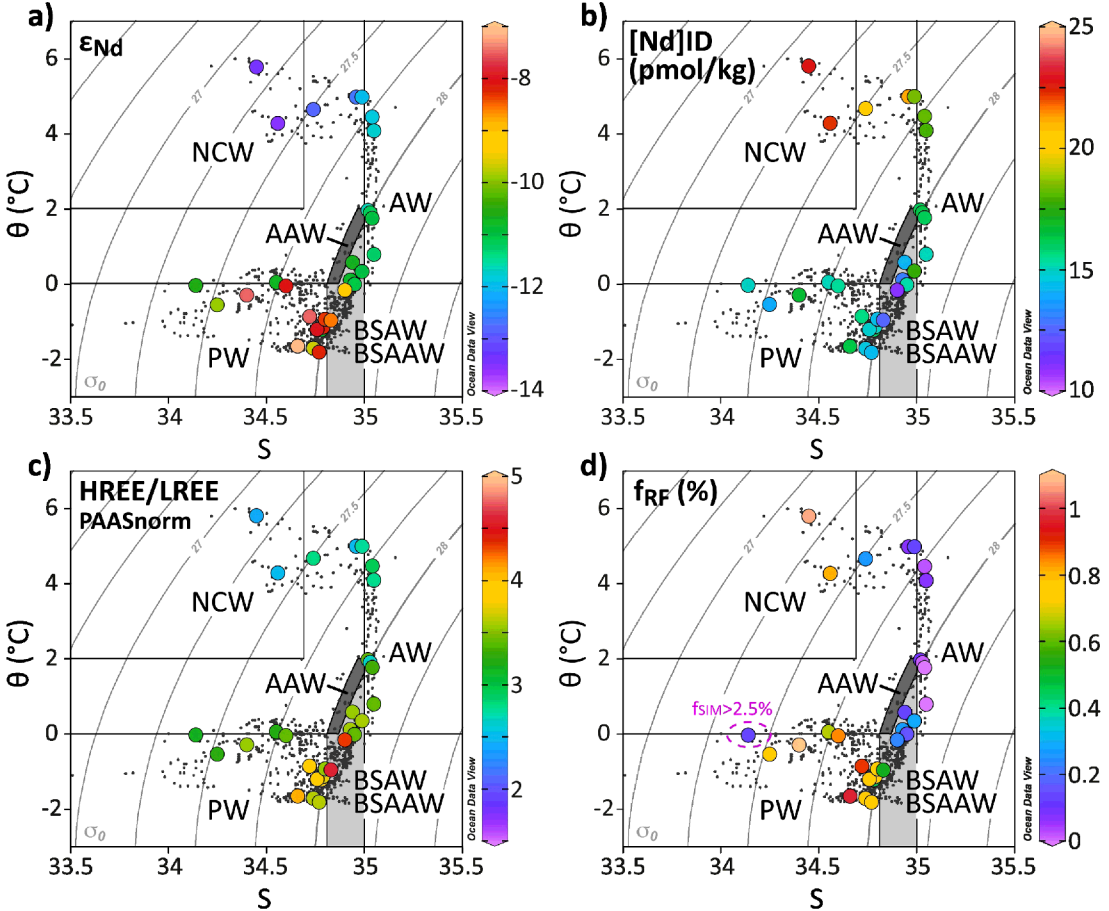
a)
εNd
b)
[Nd]ID
(pmol/kg)
c)
HREE/LREE
PAASnorm
d)
fRF (%)
fSIM>2.5%
NCW
AW
AAW
BSAW
BSAAW
PW
θ (°C)
S
σ0
Ocean Data View

Figure 2

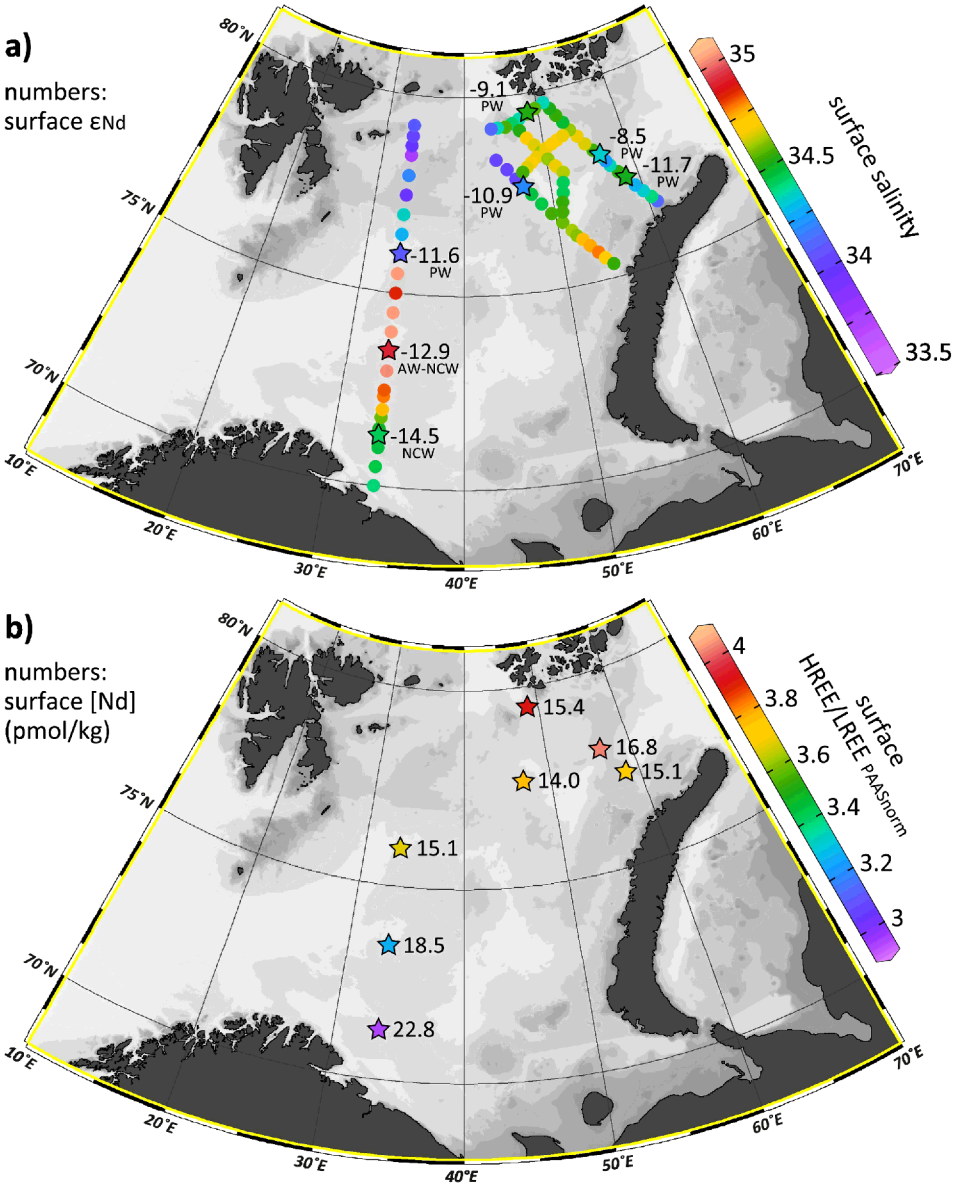
a)
numbers:
surface εNd
-9.1
PW
-8.5
PW
-11.7
PW
-10.9
PW
-11.6
PW
-12.9
AW-NCW
-14.5
NCW
surface salinity
35
34.5
34
33.5
80°N
75°N
70°N
10°E
20°E
30°E
40°E
50°E
60°E
70°E
b)
numbers:
surface [Nd]
(pmol/kg)
15.4
16.8
15.1
14.0
15.1
18.5
22.8
surface
HREE/LREE PAAsnorm
4
3.8
3.6
3.4
3.2
3

Figure 3

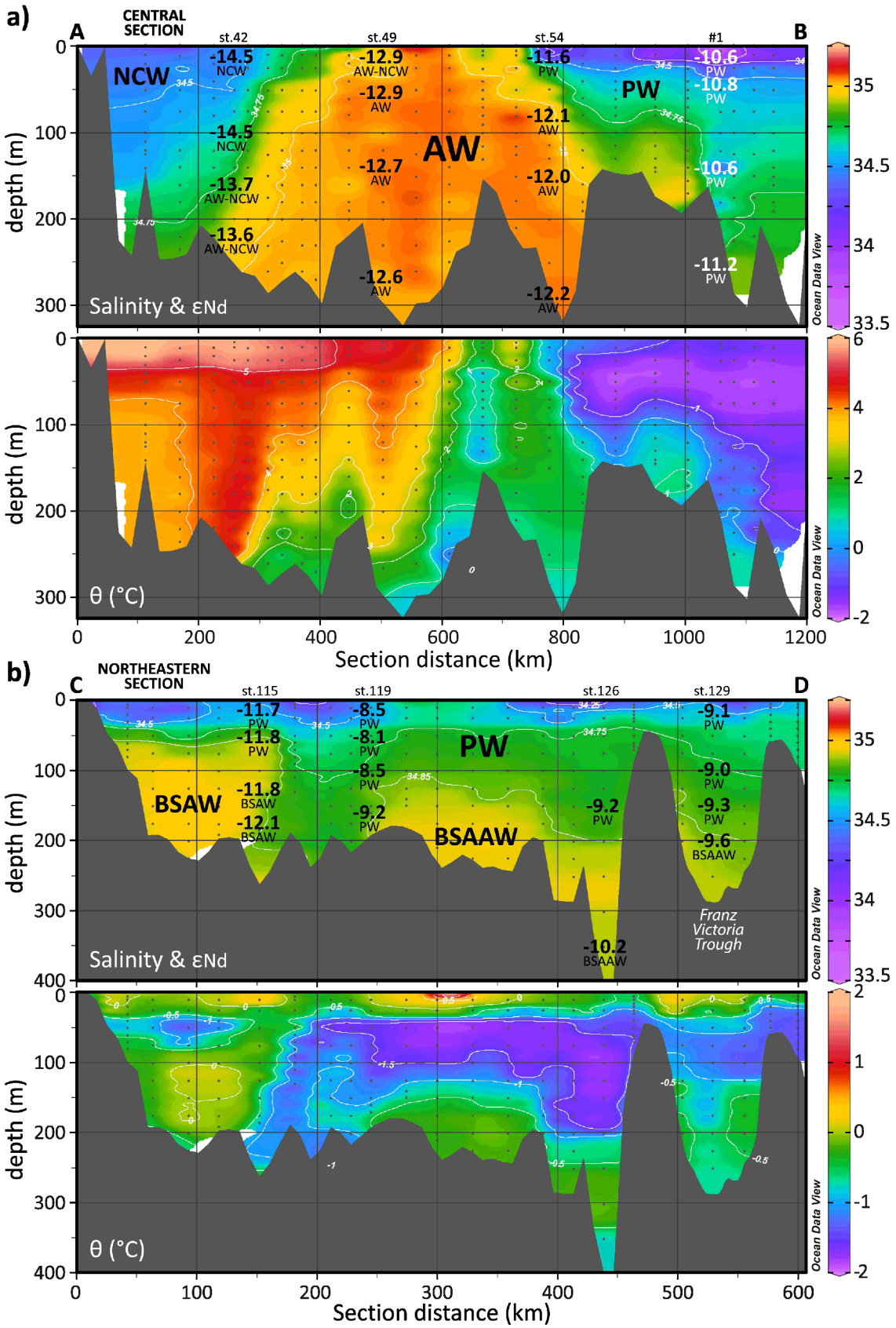
a)
CENTRAL SECTION
A
B
st.42
st.49
st.54
#1
NCW
AW
PW
-14.5 NCW
-12.9 AW-NCW
-11.6 PW
-10.6 PW
-10.8 PW
-12.9 AW
-12.1 AW
-14.5 NCW
-12.7 AW
-12.0 AW
-10.6 PW
-13.7 AW-NCW
-13.6 AW-NCW
-12.6 AW
-12.2 AW
-11.2 PW
Salinity & εNd
θ (°C)
depth (m)
Section distance (km)
Ocean Data View
b)
NORTHEASTERN SECTION
C
D
st.115
st.119
st.126
st.129
BSAW
BSAAW
PW
-11.7 PW
-11.8 PW
-8.5 PW
-8.1 PW
-9.1 PW
-8.5 PW
-9.0 PW
-11.8 BSAW
-9.2 PW
-9.2 PW
-9.3 PW
-12.1 BSAW
-9.6 BSAAW
-10.2 BSAAW
Franz Victoria Trough
Salinity & εNd
θ (°C)
depth (m)
Section distance (km)
Ocean Data View

Figure 4

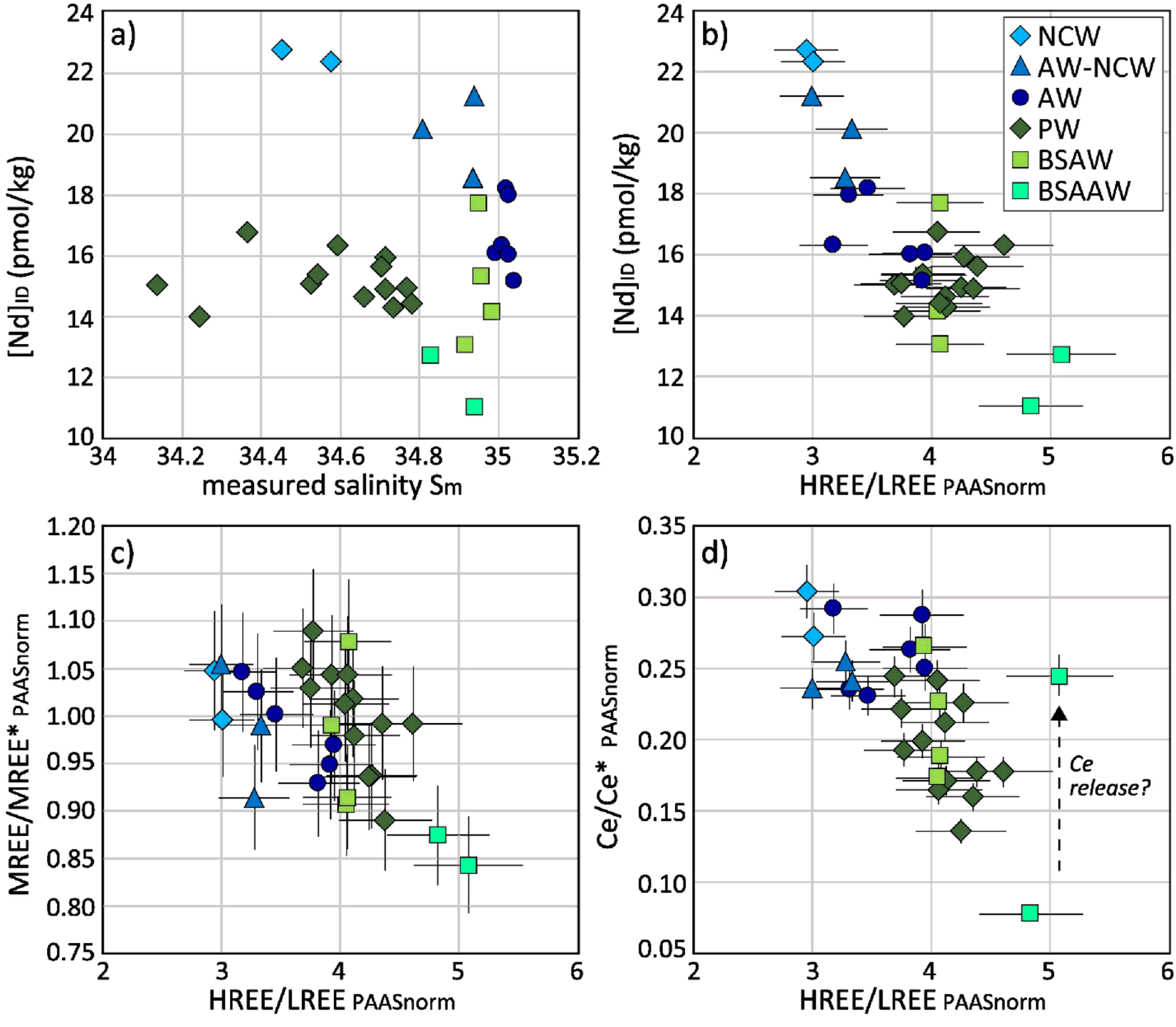
a)
b)
c)
d)
[Nd]ID (pmol/kg)
measured salinity Sm
HREE/LREE PAASnorm
MREE/MREE* PAASnorm
Ce/Ce* PAASnorm
NCW
AW-NCW
AW
PW
BSAW
BSAAW
Ce release?

Figure 5

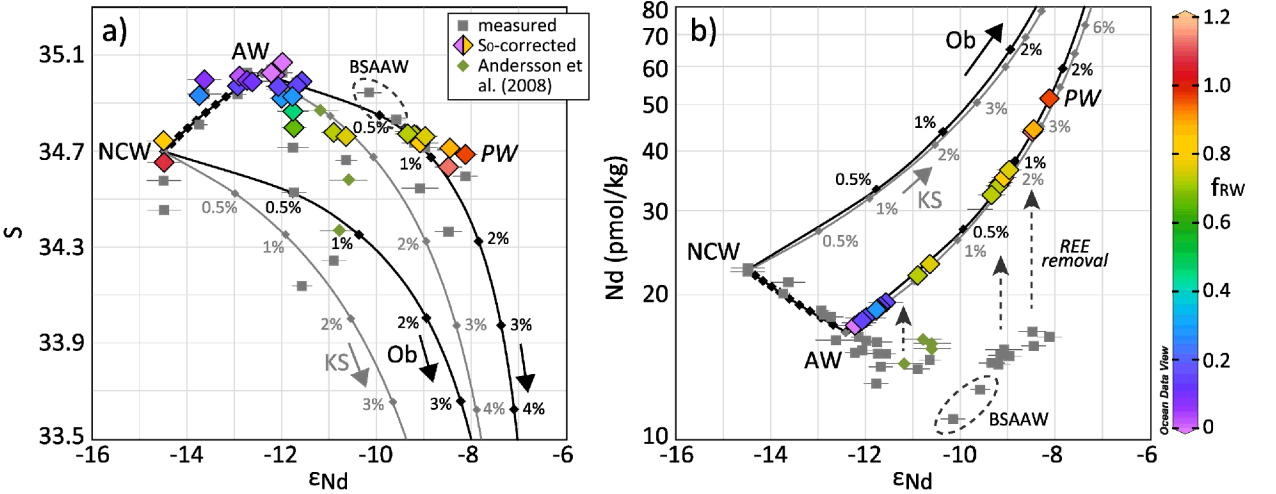
a)
measured
So-corrected
Andersson et al. (2008)
AW
BSAAW
NCW
PW
Ob
KS
0.5%
1%
2%
3%
4%
S
εNd
b)
Nd (pmol/kg)
REE removal
Ocean Data View
fRW

Figure 6

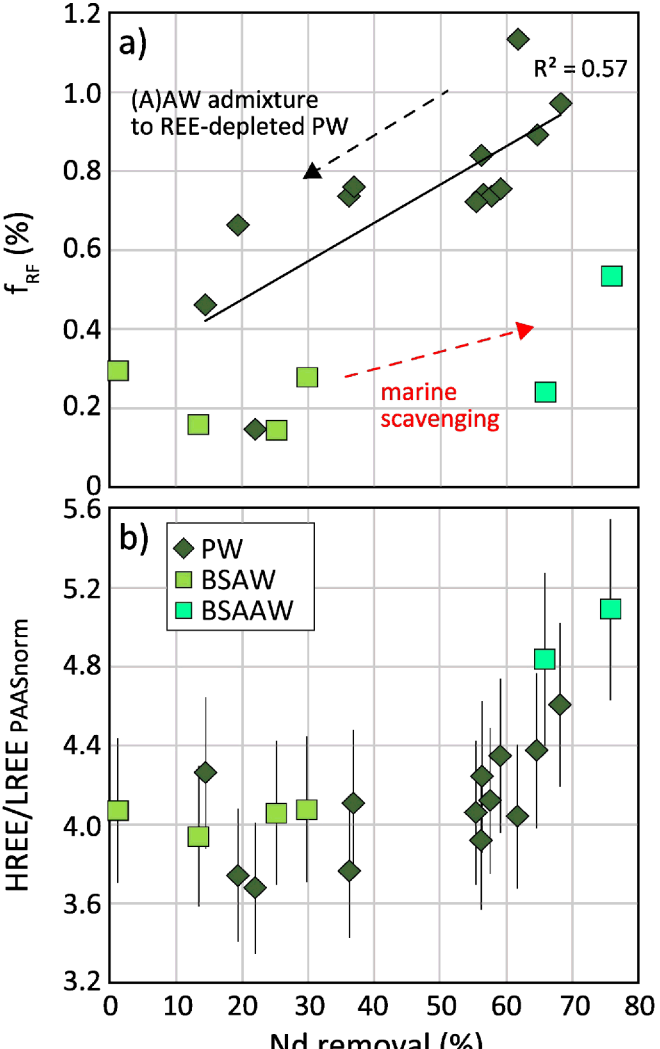
a)
(A)AW admixture
to REE-depleted PW
R² = 0.57
marine
scavenging
f_RF (%)
b)
PW
BSAW
BSAAW
HREE/LREE PAASnorm
Nd removal (%)

Figure 7